



HAL
open science

Overview of the SLOPE I and II campaigns: aerosol properties retrieved with lidar and sun–sky photometer measurements

Jose Antonio Benavent-Oltra, Juan Andrés Casquero-Vera, Roberto Román, Hassan Lyamani, Daniel Pérez-Ramírez, María José Granados-Muñoz, Milagros Herrera, Alberto Cazorla, Gloria Titos, Pablo Ortiz-Amezcuca, et al.

► To cite this version:

Jose Antonio Benavent-Oltra, Juan Andrés Casquero-Vera, Roberto Román, Hassan Lyamani, Daniel Pérez-Ramírez, et al.. Overview of the SLOPE I and II campaigns: aerosol properties retrieved with lidar and sun–sky photometer measurements. *Atmospheric Chemistry and Physics*, 2021, 21 (12), pp.9269-9287. 10.5194/acp-21-9269-2021 . hal-03320475

HAL Id: hal-03320475

<https://hal.science/hal-03320475>

Submitted on 16 Aug 2021

HAL is a multi-disciplinary open access archive for the deposit and dissemination of scientific research documents, whether they are published or not. The documents may come from teaching and research institutions in France or abroad, or from public or private research centers.

L'archive ouverte pluridisciplinaire **HAL**, est destinée au dépôt et à la diffusion de documents scientifiques de niveau recherche, publiés ou non, émanant des établissements d'enseignement et de recherche français ou étrangers, des laboratoires publics ou privés.



Overview of the SLOPE I and II campaigns: aerosol properties retrieved with lidar and sun–sky photometer measurements

Jose Antonio Benavent-Oltra^{1,2,3}, Juan Andrés Casquero-Vera^{2,3}, Roberto Román⁴, Hassan Lyamani^{2,3}, Daniel Pérez-Ramírez^{2,3}, María José Granados-Muñoz^{2,3}, Milagros Herrera⁵, Alberto Cazorla^{2,3}, Gloria Titos^{2,3}, Pablo Ortiz-Amezcuca^{2,3,6}, Andrés Esteban Bedoya-Velásquez^{3,7}, Gregori de Arruda Moreira^{3,8}, Noemí Pérez⁹, Andrés Alastuey⁹, Oleg Dubovik⁵, Juan Luis Guerrero-Rascado^{2,3}, Francisco José Olmo-Reyes^{2,3}, and Lucas Alados-Arboledas^{2,3}

¹Department of Civil, Chemical and Environmental Engineering, University of Genoa, Genoa, Italy

²Department of Applied Physics, Universidad de Granada, Granada, Spain

³Andalusian Institute for Earth System Research, IISTA-CEAMA, Granada, Spain

⁴Group of Atmospheric Optics (GOA-UVa), Universidad de Valladolid, Valladolid, Spain

⁵Laboratoire d'Optique Atmosphérique (LOA), UMR8518 CNRS, Université de Lille, Villeneuve D'ASCQ, France

⁶Institute of Geophysics, Faculty of Physics, University of Warsaw (IGFUW), Warsaw, Poland

⁷The French Aeospace Lab, ONERA, Toulouse, France

⁸Federal Institute of São Paulo (IFSP), Campus Registro, São Paulo, Brazil

⁹Institute of Environmental Assessment and Water Research (IDAEA), CSIC, Barcelona, Spain

Correspondence: Jose Antonio Benavent-Oltra (jbenavent@ugr.es)

Received: 22 January 2021 – Discussion started: 5 February 2021

Revised: 7 May 2021 – Accepted: 12 May 2021 – Published: 17 June 2021

Abstract. The Sierra Nevada Lidar aerosol Profiling Experiment I and II (SLOPE I and II) campaigns were intended to determine the vertical structure of aerosols by remote sensing instruments and test the various retrieval schemes for obtaining aerosol microphysical and optical properties with in situ measurements. The SLOPE I and II campaigns were developed during the summers of 2016 and 2017, respectively, combining active and passive remote sensing with in situ measurements at stations belonging to the AGORA observatory (Andalusian Global Observatory of the Atmosphere) in the Granada area (Spain). In this work, we use the in situ measurements of these campaigns to evaluate aerosol properties retrieved by the GRASP code (Generalized Retrieval of Atmosphere and Surface Properties) combining lidar and sun–sky photometer measurements. We show an overview of aerosol properties retrieved by GRASP during the SLOPE I and II campaigns. In addition, we evaluate the GRASP retrievals of total aerosol volume concentration (discerning between fine and coarse modes), extinction and scattering coefficients, and for the first time we present an evaluation of the absorption coefficient.

The statistical analysis of aerosol optical and microphysical properties, both column-integrated and vertically resolved, from May to July 2016 and 2017 shows a large variability in aerosol load and types. The results show a strong predominance of desert dust particles due to North African intrusions. The vertically resolved analysis denotes a decay of the atmospheric aerosols with an altitude up to 5 km a.s.l. Finally, desert dust and biomass burning events were chosen to show the high potential of GRASP to retrieve vertical profiles of aerosol properties (e.g. absorption coefficient and single scattering albedo) for different aerosol types. The aerosol properties retrieved by GRASP show good agreement with simultaneous in situ measurements (nephelometer, aethalometer, scanning mobility particle sizer, and aerodynamic particle sizer) performed at the Sierra Nevada Station (SNS) in Granada. In general, GRASP overestimates the in situ data at the SNS with a mean difference lower than $6 \mu\text{m}^3 \text{cm}^{-3}$ for volume concentration, and 11 and 2Mm^{-1} for the scattering and absorption coefficients. On the other hand, the comparison of GRASP with airborne measurements also shows an overestimation with mean absolute dif-

ferences of 14 ± 10 and $1.2 \pm 1.2 \text{ Mm}^{-1}$ for the scattering and absorption coefficients, showing a better agreement for the absorption (scattering) coefficient with higher (lower) aerosol optical depth. The potential of GRASP shown in this study will contribute to enhancing the representativeness of the aerosol vertical distribution and provide information for satellite and global model evaluation.

1 Introduction

The characterization of atmospheric aerosol optical and microphysical properties is difficult due to their high spatial and temporal variability in the atmosphere. This, together with the complexity of the aerosol–radiation interaction (scattering and absorbing incident solar and outgoing thermal radiation) and cloud–aerosol interaction (modifying cloud properties), results in a large uncertainty in the radiative forcing of climate due to aerosols (IPCC, 2013).

During the last few decades, several field campaigns have been carried out for studying atmospheric aerosol properties (e.g. Tanré et al., 2003; Mallet et al., 2016; Veselovskii et al., 2016; Vandebussche et al., 2020) using observatories with in situ measurements and that are included in global networks based on passive and active remote sensing instruments, such as the AEROSOL ROBOTIC NETWORK (AERONET; Holben et al., 1998) and European Aerosol Research Lidar NETWORK (EARLINET; Pappalardo et al., 2014). On one hand, the in situ ground-based observatories only represent a limited atmospheric sample in the layer closest to the surface. Passive remote sensing instruments, such as sun–sky photometers or satellites, provide aerosol properties in the entire atmospheric column, while they have very limited information about variations within the column. Hence, vertically resolved aerosol observations are needed to discern between the different aerosol layers and to study their radiative properties. In this regard, lidar systems are used for aerosol optical and microphysical properties profiling. Basic lidar systems only have information on the backscatter elastic signals that allow the retrieval of the aerosol backscatter coefficient (β) vertical profiles using the Klett–Fernald method (Fernald et al., 1972; Fernald, 1984; Klett, 1981, 1985) assuming a constant aerosol lidar ratio (LR). However, advanced lidar systems provide information on the backscatter elastic and inelastic signals allowing the retrieval of vertical profiles of aerosol backscatter and extinction (α) coefficients using the Raman technique (e.g. Ansmann et al., 1992; Whiteman et al., 1992). These measurements allow for the retrieval of particle vertical microphysical properties by inversion algorithms using the $3\beta + 2\alpha$ configuration (e.g. Müller et al., 1999; Böckmann, 2001; Veselovskii et al., 2002).

The main drawback of these algorithms is the scarcity of Raman lidar measurements during the daytime, which represents a limitation to the retrievals of the extinction coef-

ficient data (Veselovskii et al., 2015; Ortiz Amezcua et al., 2020). As an alternative, during the last few years, several synergetic retrievals algorithms have been developed to retrieve aerosol optical and microphysical properties combining data from sun–sky photometers and backscatter lidar measurements, such as LIRIC (Lidar-Radiometer Inversion Code) by Chaikovsky et al. (2016) and Granados-Muñoz et al. (2020) and GARRLiC (Generalized Aerosol Retrieval from Radiometer and Lidar Combined data) by Lopatin et al. (2013). One of the most popular advanced inversion algorithms is the Generalized Retrieval of Atmosphere and Surface Properties code (GRASP; Dubovik et al., 2011, 2014). It should be noted here that GARRLiC is a branch of GRASP. The versatility of GRASP allows the retrieval of aerosol vertical and surface properties combining different types of measurements, such as sun photometers, lidar, ceilometers, satellite, sky cameras, and nephelometers (e.g. Lopatin et al., 2013; Espinosa et al., 2017; Román et al., 2017; Torres et al., 2017; Benavent-Oltra et al., 2017; Titos et al., 2019; Herreras et al., 2019; Dubovik et al., 2019). The aerosol properties retrieved by GRASP have been evaluated in previous works using the volume concentration provided by the LIRIC algorithm (differences $\sim 20\%$; Benavent-Oltra et al., 2017) as reference and the backscatter and extinction coefficients calculated with Klett–Fernald and Raman methods (differences below 30% ; Benavent-Oltra et al., 2017, 2019; Tsekeri et al., 2017). In addition, the GRASP retrievals have been used to evaluate forecast models as constraints for global models and as inputs for radiative transfer models (e.g. Tsekeri et al., 2017; Chen et al., 2018, 2019; Granados-Muñoz et al., 2019). It is important to explore the potential of these kinds of algorithms by applying them to different input data and for different atmospheric conditions. In this regard, the extensive measurement dataset obtained during the Sierra Nevada Lidar aerosol Profiling Experiment I and II (SLOPE I and SLOPE II) campaigns in May, June, and July of 2016 and 2017, respectively, allows an evaluation of the atmospheric aerosol properties retrieved by the GRASP code combining lidar and sun–sky photometer measurements. This database was successfully utilized in several previous studies of the atmospheric aerosol (e.g. de Arruda Moreira et al., 2018, 2019; Bedoya-Velásquez et al., 2018; Horvath et al., 2018; Casquero-Vera et al., 2020).

The main objective of this work is to provide an overview of the aerosol optical and microphysical properties during the SLOPE I and II campaigns using the GRASP code. We checked the GRASP retrievals against the in situ measurements performed at the Sierra Nevada Station (SNS, Spain; 2500 m a.s.l.) and instrumented flights. This is the first long-term evaluation of GRASP that combines sun–sky photometer and multi-wavelength lidar measurements to retrieve profiles of aerosol intensive properties separately for both fine and coarse modes instead of only one mode such as when using ceilometer measurements (e.g. Román et al., 2018; Titos et al., 2019). In addition, a statistical analysis of both to-

tal column and vertically resolved aerosol properties is performed, and two extreme events of desert dust and biomass burning are evaluated.

2 Sites and measurements

The SLOPE I and II campaigns took place in Granada (Spain) during the summers of 2016 and 2017 and were designed to determine the vertical structure of aerosols by remote sensing instruments through the application of various retrieval schemes for obtaining aerosol microphysical and optical properties. The main objective of this campaign was to perform a closure study by comparing remote sensing system retrievals of atmospheric aerosol properties with various in situ measurements (Román et al., 2017; Benavent-Oltra et al., 2019). The study area typically presents variable aerosol loads and type, with a large presence of anthropogenic aerosols mainly in winter (e.g. Lyamani et al., 2010; del Aguila et al., 2018; Casquero-Vera et al., 2021), frequent Saharan dust intrusions (e.g. Pérez-Ramírez et al., 2012; Valenzuela et al., 2012), and primary aerosols associated with the local phenology (Cariñanos et al., 2020). The region is often affected by episodes of aerosol stagnation due to its complex geography (e.g. Lyamani et al., 2010), while Atlantic air masses are usually responsible for cleaning the atmosphere (Pérez-Ramírez et al., 2016).

During SLOPE I and II, the instrumentation was deployed at the three stations of the AGORA (Andalusian Global ObseRvatory of the Atmosphere) observatory. The main AGORA station is in the Andalusian Institute for Earth System Research/IISTA-CEAMA (UGR; 37.16° N, 3.61° W; 680 m a.s.l.) in the city of Granada. The UGR station operates many remote sensing and in situ instruments, mostly in the framework of ACTRIS (Aerosols, Clouds, and Trace gases Research InfraStructure Network, <https://www.actris.eu/>, last access: 11 June 2021) research infrastructure. The other two AGORA observatory stations are in the Sierra Nevada Mountain range Cerro Poyos (CP; 37.11° N, 3.49° W; 1820 m a.s.l.) and the Sierra Nevada Station (SNS; 37.10° N, 3.39° W, 2500 m a.s.l.). The SNS is located ~20 km south-east of Granada city and 1.8 km above the UGR station (see Fig. 1 in Herreras et al., 2019 for details). During the SLOPE field campaigns, a large set of in situ instrumentation was deployed at the SNS and on board the Partenavia P68 aircraft. The in situ measurements allowed the validation of aerosol optical and microphysical properties obtained by remote sensing techniques at the UGR station. Table 1 summarizes the main instrumentation operating at the UGR station, the SNS, and on board the aircraft.

2.1 Remote sensing instrumentation

The UGR station is equipped with a multi-wavelength Raman lidar system (LR331D400, Raymetrics S.A.), which has

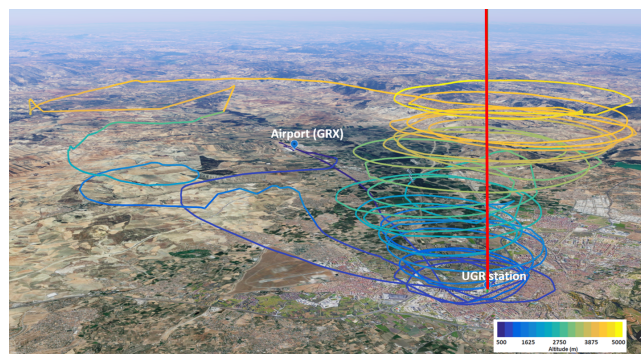


Figure 1. Map illustrating the UGR station. The coloured line indicates the trajectory of the aircraft and its altitude during the SLOPE II campaign. The red line indicates the vertical of the lidar measurements. © Google Earth.

been included in EARLINET since 2005 and contributes to the ACTRIS research infrastructure. This instrument is composed of a Nd:YAG pulsed laser that emits at 1064 nm (110 mJ per pulse), 532 nm (65 mJ per pulse), and 355 nm (60 mJ per pulse). The detection branch has seven channels: four to measure the backscattered light at 355, 532 (parallel and perpendicular components), and 1064 nm; two channels at 353.9 and 530.2 nm (387 and 607 nm until December 2016; Ortiz-Amezcuca et al., 2020) for the detection of Raman scattering from N₂, and one channel to detect the water vapour Raman scattering at 408 nm. More information on this instrument can be found in Guerrero-Rascado et al. (2008, 2009) and Ortiz-Amezcuca et al. (2020).

Each AGORA station is equipped with a sun–sky photometer CE-318 (Cimel Electronique S.A.S.) that operates in the AERONET network. This instrument performs measurements of sun direct irradiance, which is used to derive the aerosol optical depth (AOD) usually at 340, 380, 440, 500, 675, 870, and 1020 nm, and sky radiance in almucantar configuration at 440, 675, 870, and 1020 nm. The instrument at the UGR station and SNS during SLOPE I and II was the sun–sky–lunar photometer Cimel CE318-T, which also performs lunar direct irradiance measurements to retrieve the AOD during the nighttime between the first and third Moon quarters (e.g. Barreto et al. 2016, 2019; Román et al., 2020). In this work, we used AERONET Version 3 Level 1.5 (cloud-screened) data (e.g. Giles et al., 2019; Sinyuk et al., 2020).

The ground-based MWR (RPG-HATPRO G2, Radiometer physics GmbH) located at the UGR station as part of the MWRnet (Rose et al., 2005; Caumont et al., 2016) is used here for retrieving temperature profiles. MWR is a passive remote sensor that performs unattended measurements of the temperature brightness of oxygen and water vapour in the atmosphere. The oxygen is measured in the *K*-band (51–58 GHz) and the water vapour in the *V*-band from 22 to 31 GHz with a radiometric resolution between 0.3 and 0.4 rms errors at 1.0 s integration time. The retrievals of

Table 1. Instruments deployed during the SLOPE I and II campaigns at the AGORA stations.

Instrument	Location	Measurement variable	Wavelength (nm)/ nominal size range (μm)
Raman lidar system	UGR station	Elastic backscattered signal	355, 532, and 1064 nm
Sun–sky photometer	UGR, CP and SNS stations	Aerosol optical depth and sky radiances	440, 675, 870, and 1020 nm
Nephelometer TSI 3563	SNS station	Scattering coefficient	450, 550, and 700 nm
Nephelometer Aurora Ecotech	Aircraft		450, 525, and 635 nm
Aethalometer AE-33	SNS station	Absorption coefficient	370, 470, 520, and 590
Aethalometer AVIO AE-33	Aircraft		660, 880, and 950 nm
Scanning mobility particle sizer, TSI 3082	SNS station	Aitken + accumulation mode conc.	0.012–0.615 μm
Aerodynamic particle sizer, TSI 3321	SNS station	Coarse mode conc.	0.5–20 μm

temperature profiles from the measured brightness temperatures are performed using a standard feed forward neural network (Rose et al., 2005). The uncertainty of the MWR temperature profiles varies according to the weather conditions (cloud-free or cloudy), ranging between 1.8 and 3 K (Bedoya-Velásquez et al., 2019). A detailed description of this system can be found in Navas-Guzmán et al. (2014) and Bedoya-Velásquez et al. (2018, 2019).

2.2 In situ instrumentation

The integrating nephelometer (model TSI 3563) at the SNS measures the particle light scattering coefficient (σ_{sca}) at three wavelengths (450, 550, and 700 nm) with 1 min temporal resolution. The aerosol flow in the nephelometer was set to 30 L min^{-1} . The nephelometer measurements are within the angular range 7–170°, so the data were corrected for truncation and non-Lambertian illumination errors (Anderson and Ogren, 1998). The Aethalometer AE-33 (Magee Scientific Company, 206 Berkeley, USA) is based on a filter technique and provides aerosol absorption coefficients (σ_{abs}) at seven wavelengths (370, 470, 520, 590, 660, 880, and 950 nm). The aethalometer was inter-compared with other similar systems during the ACTRIS inter-comparison (ACTRIS 2 Absorption Photometer Workshop, September 2015, Leipzig, Germany), which assures the data quality. The combination of integrating nephelometer and aethalometer data allows the calculation of the aerosol extinction coefficients (α).

The scanning mobility particle sizer (SMPS) composed of an electrostatic classifier (TSI Mod. 3082) and a condensation particle counter (CPC; TSI Mod. 3772) provide the sub-micron particle number size distribution within the 6–307.5 nm particle mobility radius range with 5 min temporal resolution. SMPS data have been corrected of internal dif-

fusion losses and multiple charges by AIM software (version 10.2.0, TSI, Inc., St Paul, MN, USA). The SMPS measurements followed ACTRIS and GAW recommendations (Wiedensohler et al., 2012, 2018) and high-quality data were guaranteed after the successful participation of the instrument in the ACTRIS inter-comparisons workshops (TROPOS, Leipzig, Germany) and in situ inter-comparison (ACTRIS Round Robin Tour). The aerodynamic particle sizer (APS; TSI Mod. 3321) provides the coarse particle number size distribution within the 0.25–10 μm aerodynamic radius range. The APS also measures number aerosol concentrations up to 1000 particles cm^{-3} with coincidence errors inferior to 5 % and 10 % at 0.25 and 5 μm radius, respectively. By the combination of SMPS and APS measurements, total aerosol volume concentrations were obtained in the 0.05–10 μm radius range with 5 min time resolution. Since SMPS and APS measurement principles are based on mobility and aerodynamic particle properties, conversion from aerodynamic to mobility diameter is needed to combine both measurements. In this sense, both measurements could be related by a factor Q (Sorribas et al., 2015) that depends on chemistry and aerosol shape. Due to the absence of information of both properties, Q -value = 1 has been assumed for conversion from aerodynamic to mobility size distribution (mobility diameter equal to aerodynamic diameter).

2.3 Aircraft instrumentation

During the campaigns, dedicated flights with an aircraft (Partenavia P68) equipped with in situ instrumentation were carried out over the study area between 15 and 18 June 2016 for the SLOPE I campaign and between 21 and 24 June 2017 for the SLOPE II campaign. The aircraft campaigns consisted of three flights each year. Figure 1 shows the spiral trajectories of one flight; each flight consisted of several as-

ending and descending spiral profiles centred on the location of the UGR station. The radius of the spirals were about 500 m. On each flight, only ascending profiles were used in the following analysis. To avoid the potential partial sampling of the exhaust of the aircraft, the descending profiles were performed at a different location.

Air flows to the instruments through a near-isokinetic isoaxial inlet designed by Aerosol d.o.o. (<https://www.aerosol.si>, last access: 11 June 2021) at a flow rate of 10 L min^{-1} . The main flow is divided by two flow splitters that divide the sampled air among the instruments. Yus-Díez et al. (2021) reported minimal losses in the inlet system for small particles, while larger differences were observed for particles with radius $> 2\text{--}2.5 \mu\text{m}$. The Ecotech Aurora nephelometer is an integrating nephelometer that measures the particle light scattering coefficient at three wavelengths (450, 525, and 635 nm) with a time resolution of 10 s. This instrument measures the scattering coefficient in the angular range $10\text{--}170^\circ$, and the correction of Müller et al. (2011) was used to account for the angular truncation errors. The Aethalometer AVIO AE33 (Aerosol d.o.o.) is the aircraft version of the Aethalometer AE-33 described above. Using the same measurement principle (Drinovec et al., 2015), it provides particle absorption coefficients at seven wavelengths (370, 470, 520, 590, 660, 880, and 950 nm) with a time resolution of 1 s. The position of the aircraft was tracked using GPS and all instruments on board the aircraft were time synchronized. Further information on the aircraft instrumentation can be found in Yus-Díez et al. (2021).

3 Methodology

3.1 GRASP retrievals

In this work, we use the GRASP code following the scheme proposed by Lopatin et al. (2013), which combines lidar and sun–sky photometer measurements to retrieve the optical and microphysical properties of aerosol particles. This scheme uses normalized backscattered range corrected signal at 355, 532, and 1064 nm from lidar, the AOD, and sky radiance (almucantar scan) both at 440, 675, 870, and 1020 nm from AERONET version 3 level 1.5. It should be noted that the GRASP retrievals were performed during the daytime with solar zenith angles larger than 40° and clear-sky conditions. This configuration of GRASP allows the retrieval of aerosol properties for both fine (radii range 0.05 to $0.576 \mu\text{m}$) and coarse (radii range 0.33 to $15 \mu\text{m}$) modes separately, the complex refractive index, single-scattering albedo (SSA), and lidar ratio (LR). In addition, GRASP provides vertical concentration of fine and coarse mode separately, and the vertically resolved profiles of the extinction, absorption, and scattering coefficients, SSA, LR, Ångström exponent of absorption (AAE), and scattering (SAE).

Individual GRASP retrievals are performed for each sky radiance almucantar sequence available from AERONET with correlative lidar measurements in a $\pm 15 \text{ min}$ time window. Specifically, the normalized lidar range corrected signal profile used in each retrieval was previously 30 min averaged and computed for 60 log-spaced heights between the minimum and maximum heights as proposed by Lopatin et al. (2013). Here, the minimum height has been chosen as 400 m above the ground to minimize the effect of incomplete overlap and the maximum height as 6000 m above the ground to have a higher signal-to-noise ratio. This GRASP configuration is described in detail in Benavent-Oltra et al. (2019). The data used in this study were recorded between May and July of 2016 and 2017 with 286 retrievals in 69 d that passed the filter imposed to the inversion process (relative residual $< 15 \%$; Torres et al., 2017).

3.2 Aircraft data

In order to make comparable the profiles from the aircraft data and the remote sensing retrievals, there are some corrections to consider. Remote sensing data are provided at ambient conditions (temperature and pressure), but the aircraft data are registered at different conditions. Nephelometer data from the aircraft were recorded at cabin temperature and ambient pressure, and aethalometer data were registered at 0°C and 1013.25 hPa. The cabin temperature used was the nephelometer sampling temperature (T_s), i.e. the temperature inside the nephelometer, and the profile atmospheric pressure used was the nephelometer pressure sensor (P_s). The cabin on the aircraft was not pressurized so the pressure inside the nephelometer can be considered the outside pressure. The aircraft did not register the outside temperature, so an external source of temperature profile was required. We used a temperature profile from a microwave radiometer MWR (T_{mwr}) as described in Sect. 2.1 using an average profile during the time of the entire aircraft profile and interpolated to the exact altitudes of the aircraft profile.

Aircraft profiles show some noise, especially at higher altitudes, so a convolution with a mean filter was applied to the aircraft in situ data in order to smooth the profiles. We observed that using 100 m for the nephelometer and 200 m for the aethalometer data in the vertical profiles reduced noise while preserving the profile features. Finally, Aurora nephelometer wavelengths were converted to the TSI wavelengths using the Ångström exponent law to make the aircraft and ground based in situ data comparable.

4 Results

4.1 Evaluation of the GRASP retrievals versus in situ data

4.1.1 At the high mountain station

For the inter-comparison between the GRASP retrievals and the SNS in situ data, we selected the in situ measurements averaged in ± 15 min around the GRASP retrieval time and the 400 m averaged data of the GRASP retrieval profile at 2500 m a.s.l. (SNS altitude). The number of coincident GRASP retrievals with in situ measurements are 231, 202, 154, and 151 for volume concentration, σ_{sca} , σ_{abs} , and α coefficients, respectively. Therefore, the results and discussion about the comparison between the GRASP and the SNS in situ measurements refer exclusively to this height range.

Figure 2 shows the aerosol total (VC_{T}), fine mode (VC_{F}), and coarse mode (VC_{C}) volume concentration retrieved by GRASP versus those measured with in situ instruments at the SNS. The aerosol volume concentrations at the SNS were calculated for the 0.05–0.5 and 0.5–10 μm radius size ranges for the fine and coarse modes, respectively. Due to the sensitivity of linear regression to outliers, VC_{T} concentrations larger than 190 $\mu\text{m}^3 \text{cm}^{-3}$ (99 percentile) and their corresponding fine and coarse data have been excluded in this analysis. In general, volume concentrations retrieved by the GRASP code show good correlation with the SNS measurements with correlation coefficients (R) of 0.58, 0.83, and 0.80 for fine, coarse, and total volume concentrations, respectively. The results show that the GRASP retrievals overestimate in situ measurements with a mean difference (\pm standard deviation) of 4 ± 4 and $6 \pm 8 \mu\text{m}^3 \text{cm}^{-3}$ for fine and total volume concentrations, respectively. In contrast, better correlation is observed for coarse mode volume concentrations (slope equals 1) with a lower mean difference ($2 \pm 6 \mu\text{m}^3 \text{cm}^{-3}$). In terms of absolute concentrations, 65 % (91 %), 70 % (88 %), and 45 % (71 %) of the differences are observed within $\pm 5 \mu\text{m}^3 \text{cm}^{-3}$ ($\pm 10 \mu\text{m}^3 \text{cm}^{-3}$) for fine, coarse, and total volume concentrations, respectively. These results are similar to those found in previous GRASP assessments by Benavent-Oltra et al. (2017) and Tsekeri et al. (2017). These authors also showed an overestimation of VC_{F} compared with in situ data, while for VC_{C} , similar GRASP retrievals to in situ data were found for cases where coarse particles are predominant. The observed overestimation is lower than the obtained by Román et al. (2018) using GRASP with ceilometer data and by Benavent-Oltra et al. (2019) using GRASP with lidar emission signals at 355, 532, and 1064 nm. Titos et al. (2019) found that the agreement between the GRASP retrievals (from ceilometer measurements) and in situ data improved when the contribution of fine particles was negligible.

Figure 3 shows σ_{sca} and σ_{abs} obtained by GRASP at ~ 2.5 km height versus those obtained by in situ measure-

ments at the SNS. The comparison was performed by interpolating the GRASP values at 355, 532, and 1064 nm to the wavelengths of the nephelometer (450, 550, and 700 nm) and the aethalometer (370, 520, and 880 nm) using the Ångström exponent law. For σ_{sca} , we can observe that generally the agreements between GRASP and in situ data are similar at the three wavelengths ($R \sim 0.95$). The slopes of the linear fits are equal to 1 with an intercept lower than 10 Mm^{-1} that decreases for larger wavelengths. Globally, GRASP overestimates in situ data at the SNS with a mean difference (\pm standard deviation) of 11 ± 17 , 6 ± 14 , and $4 \pm 11 \text{ Mm}^{-1}$ at 450, 550, and 700 nm, respectively. On the other hand, for σ_{abs} , GRASP shows good correlation with the in situ data with correlation coefficients around 0.85. In general, GRASP overestimates the in situ data at the SNS as shown by the slopes (~ 1.2) and intercepts (from 0.5 to 1.5 Mm^{-1}) of the regressions. The mean differences (\pm standard deviation) of σ_{abs} are 2 ± 6 , 1 ± 3 , and $0.8 \pm 1.7 \text{ Mm}^{-1}$ at 370, 520, and 880 nm, respectively. Furthermore, the differences between GRASP and in situ measurements are less than $\pm 2.5 \text{ Mm}^{-1}$ for 61 %, 81 %, and 90 % of the data at 370, 520, and 880 nm, respectively. The results from Fig. 3 for the validation of σ_{sca} are similar to previous validations of the GRASP retrievals with in situ data from high mountain sites (e.g. Titos et al., 2019; Benavent-Oltra et al., 2019). However, it should be noted that the results presented here are the first direct validation of retrieved σ_{abs} .

Finally, the comparison between the GRASP retrievals and in situ data for the extinction coefficient at 532 nm showed evidence of better agreement (Fig. 4a). The in situ extinction coefficient at 532 nm is the sum of the scattering and absorption coefficients interpolated to 532 nm using the Ångström exponent law. The GRASP retrievals and in situ data show good agreement (slope equals 1) and are highly correlated ($R = 0.9$). Figure 4b shows the frequency histogram of the differences in extinction coefficient ($\Delta\alpha$) between GRASP and in situ, showing a skewed histogram to positive differences that implies slight overestimation by GRASP. These overestimations can be associated with the differences in scattering coefficient.

4.1.2 Aircraft profiles

A total of six flights were carried out on 15, 17, and 18 June 2016 during SLOPE I and 21, 23, and 24 June 2017 during SLOPE II. During the SLOPE I flights, the aerosol conditions were characterized by AOD values at 440 nm (AOD_{440}) lower than 0.1 and an Ångström exponent (AE), computed with AOD at 440 and 870 nm ($\text{AE}_{440-870}$), between 0.6 and 1.3. On the other hand, during the week of flights for SLOPE II, there was a dust intrusion from the Sahara with higher AOD_{440} values (ranging from 0.13 to 0.36 on 23 and 24 June 2017, respectively) and low $\text{AE}_{440-870}$ values between 0.3 and 0.8. Figure 5 shows the vertical profiles of scattering and absorption coefficients retrieved by the

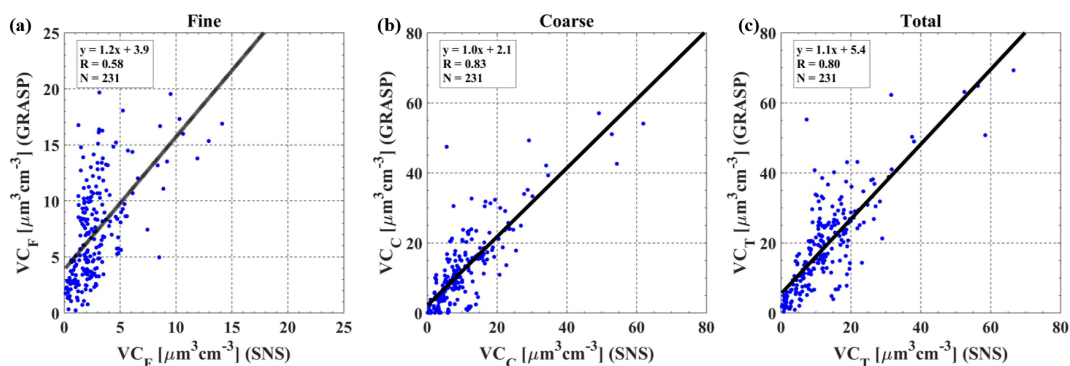


Figure 2. Volume concentration (VC) retrieved by GRASP at the SNS height versus in situ measurements at the SNS for (a) fine, (b) coarse, and (c) total modes.

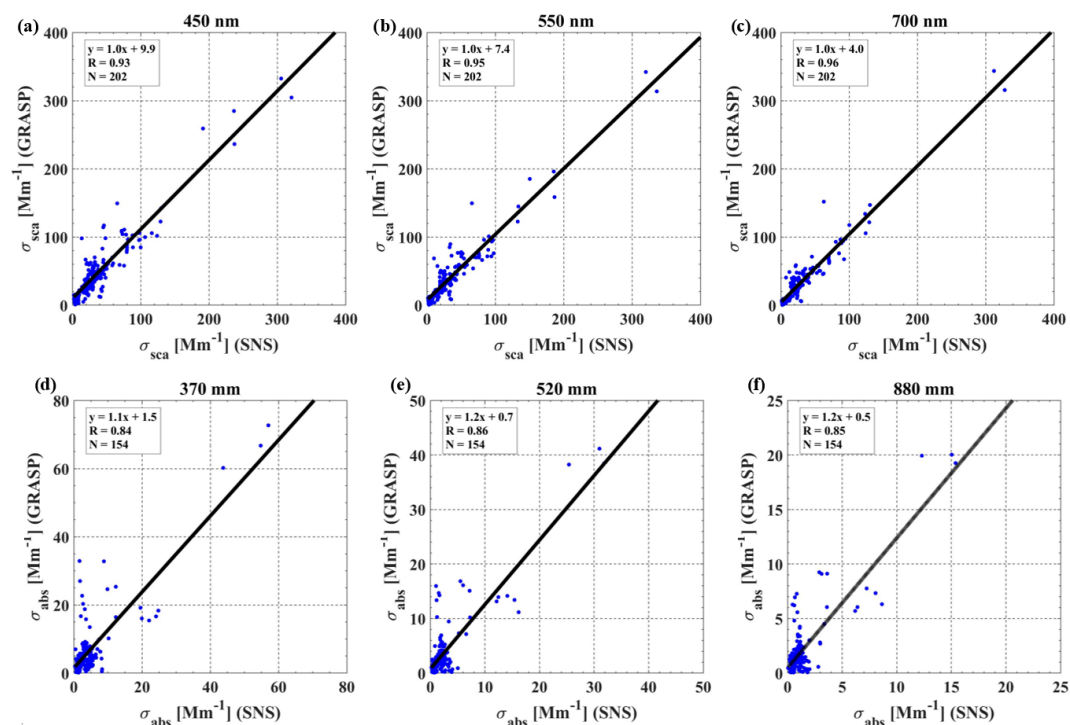


Figure 3. (a, b, c) Scattering (σ_{sca}) and (d, e, f) absorption (σ_{abs}) coefficients retrieved by GRASP at the SNS height versus in situ measurements at the SNS.

GRASP code and measured by the on-board instrumentation. This figure also includes the mean value measured at the SNS during the flights. For the sake of comparison, the GRASP values at 355, 532, and 1064 nm have been interpolated to the nephelometer and aethalometer wavelengths using the Ångström exponent law.

For σ_{sca} , both GRASP and airborne measurements follow the same pattern where GRASP overestimates the airborne data with a mean absolute difference of $14 \pm 10 \text{ Mm}^{-1}$. During SLOPE I, these mean absolute differences are lower than 8 Mm^{-1} and there is a good agreement between GRASP and the SNS measurements (differences $< 4 \text{ Mm}^{-1}$). How-

ever, during SLOPE II, the differences between GRASP and in situ measurements (both airborne and SNS) are larger, reaching values of 30 Mm^{-1} . In the case of σ_{abs} , the GRASP and airborne profiles show large differences during SLOPE I with mean absolute differences between 0.5 and 3 Mm^{-1} and reaching differences around 6 Mm^{-1} on 18 June 2016. On the other hand, the absorption coefficients retrieved by GRASP show good agreement with in situ measurements (both airborne and SNS) with a mean absolute difference of $0.7 \pm 0.4 \text{ Mm}^{-1}$ during SLOPE II. In general, the differences between GRASP and in situ measurements are close to the detection limit for the aethalometer on board the aircraft and

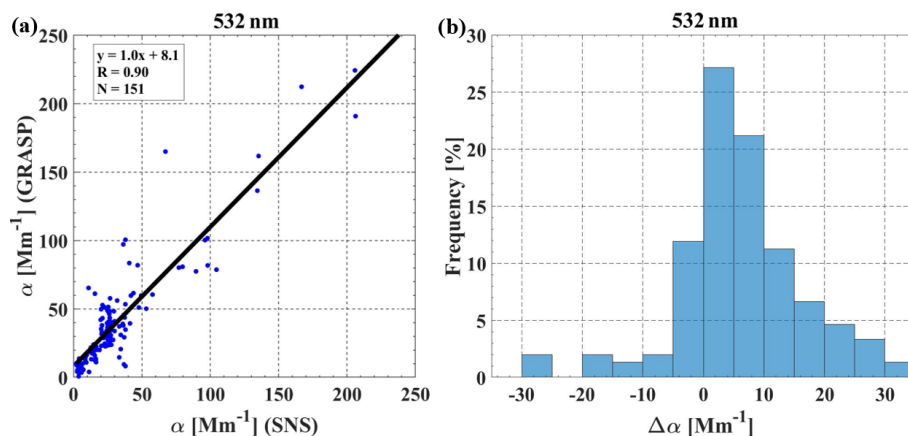


Figure 4. (a) Extinction (α) coefficient retrieved by GRASP at the SNS height versus the in situ measurements at the SNS and (b) the histogram of the absolute difference between GRASP and the SNS in situ measurements.

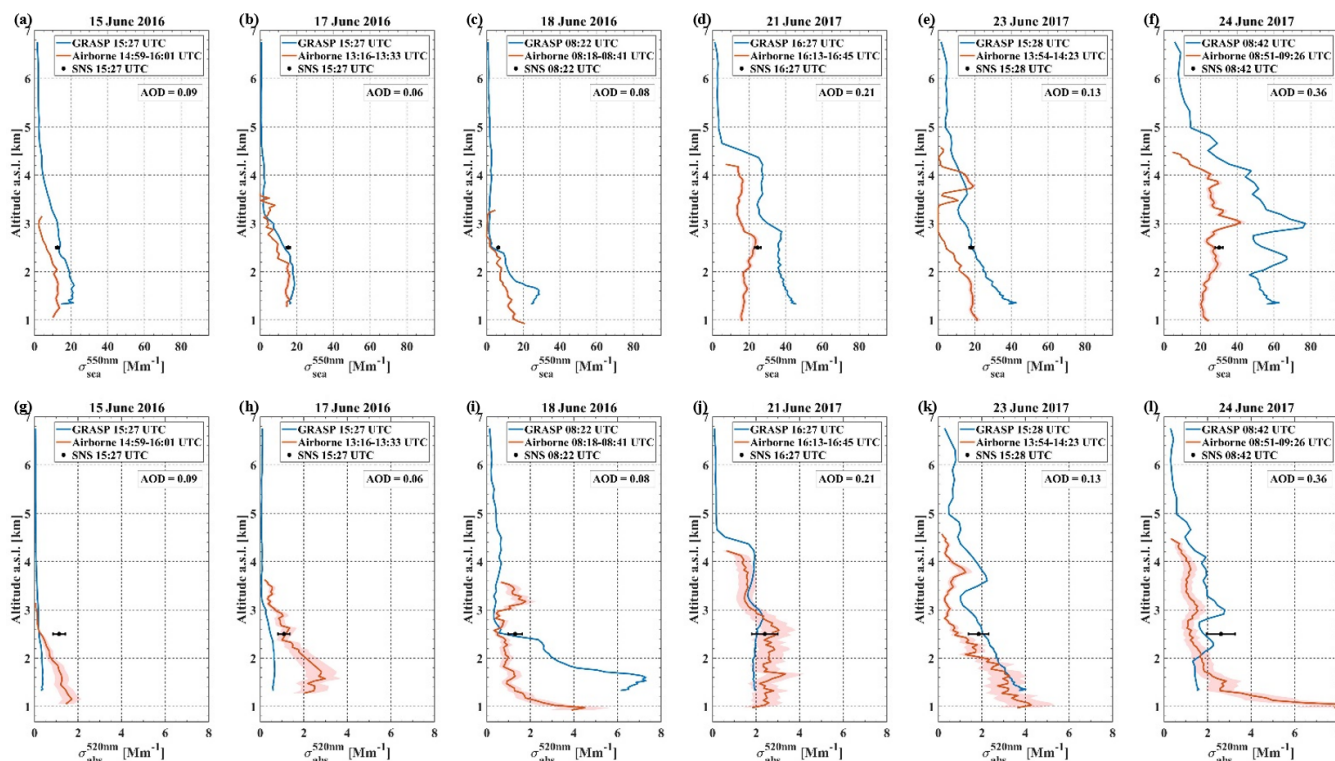


Figure 5. Scattering (σ_{sca}) and absorption (σ_{abs}) coefficients at 520 nm retrieved by GRASP (blue), aircraft (red), and the SNS (black) in situ measurements on (a, g) 15, (b, h) 17, and (c, i) 18 June 2016 and (d, j) 21, (e, k) 23, and (f, l) 24 June 2017. The AOD shown is at 440 nm.

the SNS. The differences obtained both for σ_{sca} and σ_{abs} can be explained due to the low AOD_{440} (below 0.40), which represents a challenge for the retrieval of the aerosol properties both for AERONET (Dubovik and King, 2000; Dubovik et al., 2000) and inversion algorithms such as GRASP (Lopatin et al., 2013). However, the very good agreement in absorption coefficient during SLOPE II indicates the good capability of GRASP to retrieve vertical profiles of absorption to AOD_{440} higher 0.1.

4.2 Aerosol properties during SLOPE I and II

4.2.1 Column integrated

Figure 6 shows the temporal evolutions of AOD_{440} and $\text{AE}_{440-870}$ daily mean values retrieved by the GRASP code at the UGR station during the SLOPE I and II campaigns. Daily averaged values of AOD_{440} retrieved by the GRASP code range from 0.06 to 1.0 with a mean (\pm standard deviation)

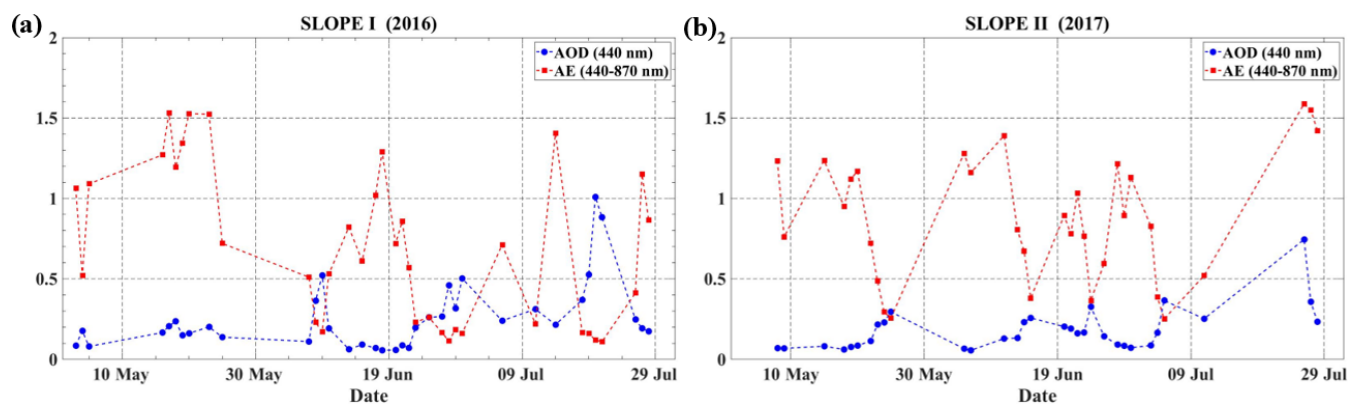


Figure 6. Temporal evolution of aerosol optical depth (AOD) at 440 nm and Ångström exponent (440–870 nm) retrieved by GRASP during the (a) SLOPE I and (b) SLOPE II campaigns.

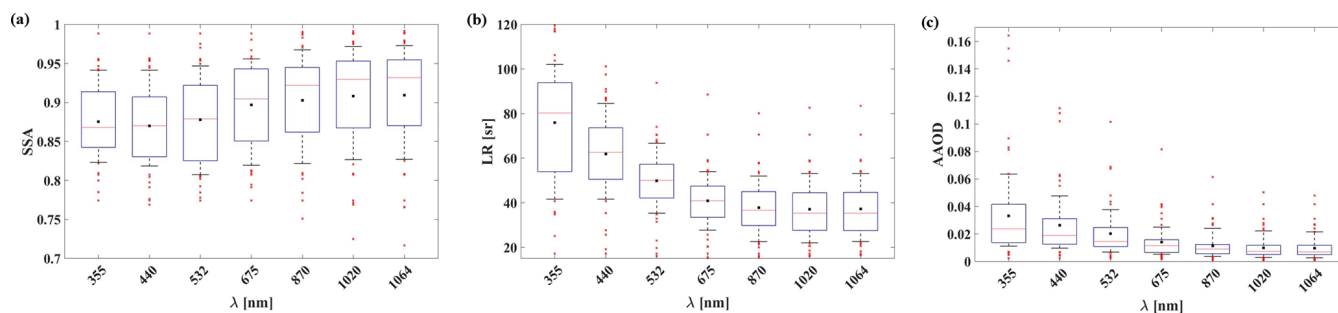


Figure 7. Statistics of (a) single-scattering albedo (SSA), (b) lidar ratio (LR), and (c) absorption aerosol optical depth (AAOD), at 355, 440, 532, 675, 870, 1020, and 1064 nm retrieved by the GRASP code during the SLOPE I and II campaigns represented as box diagrams. In these box diagrams, the mean is represented by a black dot and the line segment in the box is the median. The bottom and top edges of the box indicate the 25th and 75th percentiles, respectively. In addition, the error bars of the box are the 10th and 90th percentiles and the crosses represent the outliers.

tion) value of 0.22 ± 0.18 , while $AE_{440-870}$ varies from 0.11 to 1.6 with a mean value of 0.8 ± 0.4 . The large variability of the AODs and Ångström exponents observed in Fig. 6 are typical for this season in the study area (e.g. Pérez-Ramírez et al., 2012). Large AODs and low AE values like those observed on 20 July 2016 are related to Saharan dust outbreaks (e.g. Román et al., 2018; Benavent-Oltra et al., 2019), while large AODs and AE values like those observed on 26 July 2017 are related to biomass burning transport (from Portugal in this case) (Turco et al., 2019).

Figure 7 shows the box-and-whisker diagrams of retrieved aerosol columnar-integrated properties such as SSA, LR, and aerosol absorption optical depth (AAOD) at 355, 440, 532, 675, 870, 1020, and 1064 nm retrieved by the GRASP code during the study period. For aerosol intensive properties, the SSA values are typical for Saharan dust outbreaks at the study region (e.g. Valenzuela et al., 2012), ranging from 0.88 ± 0.05 at 355 nm to 0.90 ± 0.06 at 1064 nm, respectively. These relatively large values of SSA for all wavelengths indicate a small concentration of absorbing aerosol particles (e.g. mineral dust). The LR values show large wave-

length variability with mean values ranging from 80 ± 30 sr at 355 nm to 35 ± 16 sr at 1064 nm, which are typical for Saharan dust (Shin et al., 2018). For aerosol extensive properties, the highest AAODs (> 0.10) correspond both to dust and biomass-burning events, with an absorption Ångström exponent (AAE; computed in the spectral range 355–1064 nm) higher than 1.5 for the desert dust event and around 1.0 for the biomass burning event. The variability in AAE can be explained by the differences in particle chemical compositions (e.g. Russell et al., 2010; Cazorla et al., 2013; Liu et al., 2018), but in the context of the current capabilities of the GRASP retrievals, we could not advance with such analyses. Nevertheless, GRASP revealed a small contribution of aerosol absorption in the total aerosol optical depth during the SLOPE I and II field campaigns even for cases with relatively low AODs.

The large standard deviations and percentiles observed in Fig. 7 for all aerosol optical properties agree with the variability of aerosol types deduced from Fig. 6. The aerosol variability can be caused by the fact that different air masses reach the south-east of Spain. Usually, the air

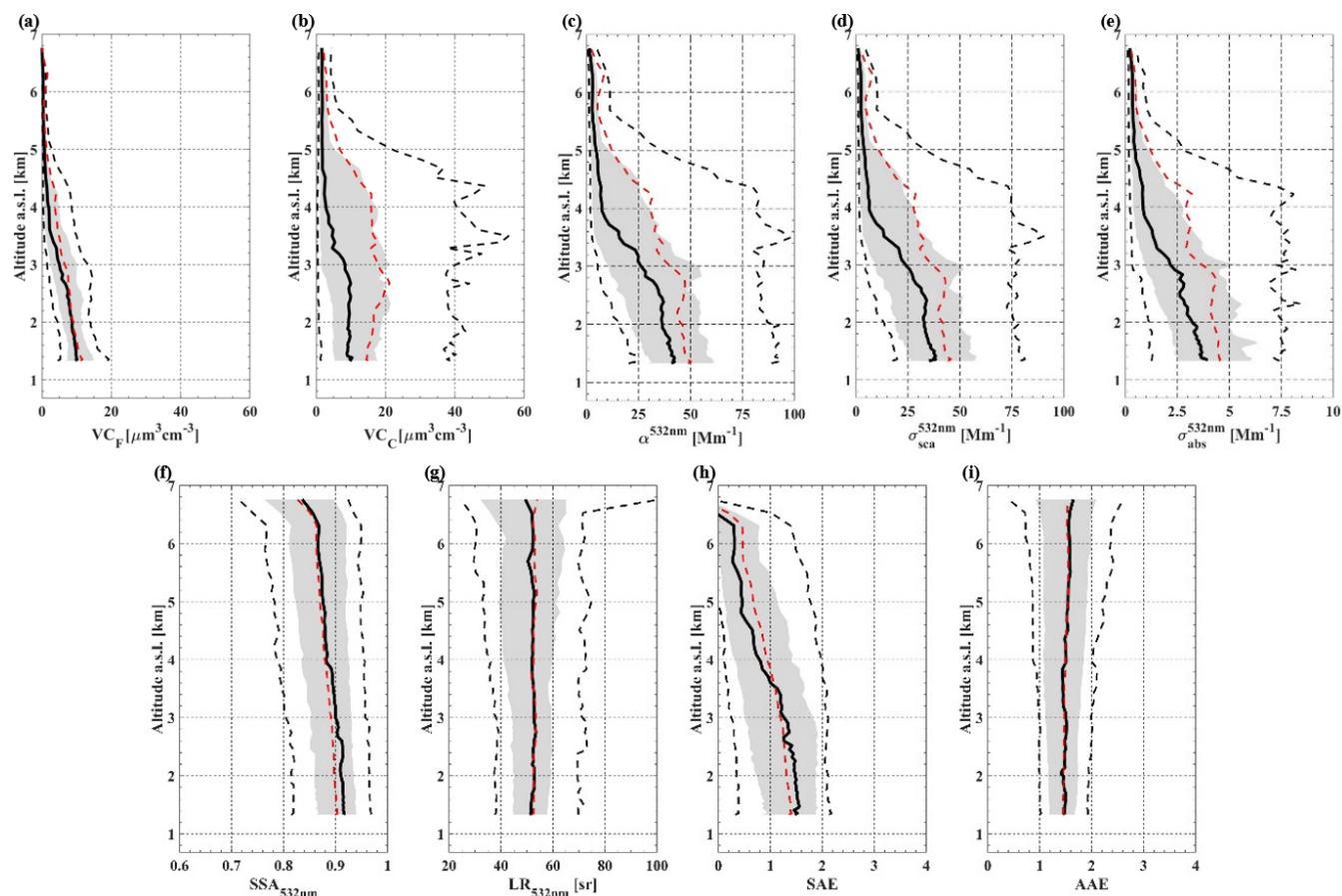


Figure 8. Variability of the GRASP vertical profiles. Volume concentration for (a) fine and (b) coarse modes. (c) Extinction (α), (d) scattering (σ_{sca}), and (e) absorption (σ_{abs}) coefficients. (f) Single-scattering albedo (SSA) and (g) lidar ratio (LR) at 532 nm. (h) Scattering Ångström exponent (SAE) and (i) absorption Ångström exponent (AAE) computed between 355 and 1064 nm. The black line represents the median and the red dashed line is the mean. The shaded area is the interquartile range and the black dashed lines represent the 10th and 90th percentiles. Statistics are based on daily average profiles.

masses in the study region come from the Atlantic bringing clean air, or from north of Africa transporting mineral dust, or from the Mediterranean transporting anthropogenic particles (e.g. Pérez-Ramírez et al., 2016). Another frequent source of aerosol particles are the biomass burning events near the study region (Alados-Arboledas et al., 2011; Ortiz-Amezua et al., 2017; Sicard et al., 2019). According to the natural aerosol episode warning system from MITECO (Spanish Ministry for Ecological Transition and Demographic Challenge, <https://www.miteco.gob.es/es/calidad-y-evaluacion-ambiental/temas/>, last access: 1 June 2020), on around 66 % and 10 % of the evaluated days with the GRASP retrievals there were associated North African intrusions and biomass burning events in the south-east of Spain, respectively.

4.2.2 Vertically resolved

Figure 8 shows a statistical overview of the aerosol optical and microphysical properties profiles retrieved by

GRASP: volume concentration, differentiating between fine and coarse mode, and for the aerosol optical properties the extinction, scattering, and absorption coefficients plus SSA and LR, all at the reference wavelength of 532 nm. Additionally, we include the AAE and SAE computed between 355 and 1064 nm. As mentioned in Sect. 3.1., a total of 286 GRASP retrievals passed the filter imposed. For the statistical overview, we compare point by point the 60 log-spaced heights of each aerosol property profiles. The solid black lines represent the medians and red dashed line the means. The shaded area is the interquartile range and the black dashed lines represent the 10th and 90th percentiles.

For aerosol microphysical properties (Fig. 8a, b) we observe an approximately linear decay with altitude until they reach approximately zero at 4–5 km a.s.l. The largest values are at the lowest altitudes (with average $\sim 10 \mu\text{m}^3 \text{cm}^{-3}$). The VC_F profile shows lower variability (a smaller interquartile range) than the VC_C profile. The highest variability in the coarse particles profile, which is the 90th percentile with val-

ues between 40 and $60 \mu\text{m}^3 \text{cm}^{-3}$, is mainly caused by the intrusion of desert dust particles during the SLOPE I and II campaigns.

The extinction, scattering and absorption coefficient profiles at 532 nm (Fig. 8c, d, e) show similar behaviour as VC profiles. These patterns of extinction coefficient profiles for long-term statistical analyses have been observed in Europe for previous studies using Raman lidar data (e.g. Amiridis et al., 2005; Navas-Guzmán et al., 2013). The largest values for the particle extinction, scattering, and absorption coefficients are observed for the altitudes below 2 km a.s.l. (40, 35, and 4Mm^{-1} for α , σ_{sca} , and σ_{abs} , respectively). This behaviour of the σ_{sca} profile has been previously observed in other statistical lidar studies (e.g. Titos et al., 2019). The SSA profile at 532 nm decreases with values from 0.92 at the lowest altitude to 0.86 at the highest altitude and with interquartile range ~ 0.025 , which is close to the uncertainties claimed for SSA retrievals using remote sensing techniques (e.g. Pérez-Ramírez et al., 2019). The combination of σ_{abs} and SSA reveals that for the entire profile approximately 10 % of the total extinction corresponds to absorption. Thus, the GRASP retrievals show the capability of this code to characterize aerosol absorption coefficients with vertical resolution, which is a step towards aerosol characterization.

The profiles of intensive properties such as LR, AAE, and SAE can provide information about the predominance of different aerosol particle types. For LR at 532 nm (Fig. 8g), a constant mean profile is observed with a mean value of ~ 52 sr. LR at a given wavelength depends mainly on both chemical composition and particle shapes (Müller et al., 2007), which explains the variability in the retrieved values for the different aerosol types with a strong contribution of mineral dust. The LR values obtained are very similar to those observed in other studies (e.g. Guerrero-Rascado et al., 2009; Navas-Guzmán et al., 2013a). For SAE (Fig. 8h), which is more related to the predominant particle size, the highest value is found at the lowest altitude, suggesting larger predominance of fine particles closer to the surface. This pattern agrees with the assumption of higher anthropogenic aerosol loads at these altitudes, which are dominated by fine-mode particles. Furthermore, it agrees with the low mixture of transported mineral dust with anthropogenic pollution at altitudes above the atmospheric boundary layer top. Finally, AAE (Fig. 8i), which is related to the chemical composition of the absorbing aerosol, follows a constant pattern with altitude with a mean value of ~ 1.45 with the 10th and 90th percentiles equal to 1 and 2, respectively. These are the values typically found for Saharan mineral dust particle transport and their mixture with anthropogenic pollutants (Russell et al., 2010).

4.2.3 Special events

During the SLOPE I and II campaigns two extreme events occurred with $\text{AOD}_{440} \sim 1.0$. The first one was a Saharan

mineral dust outbreak (DD) in July 2016, and the second was a biomass burning transport event (BB) in July 2017 with fires originating in Portugal. Figures 9 and 10 show the profiles of aerosol optical and microphysical properties for the DD and BB events, respectively. Also included in these figures is the time when retrievals were obtained, the AOD at each moment, and the SNS measurements at the available periods.

Figures 9 and 10 show that for the first day of each event (20 July 2016 and 26 July 2017) decoupled aerosol layers were observed at approximately ~ 4 km a.s.l. Such decoupled layers went gradually downward until they reached the altitude of ~ 2 – 3 km a.s.l. in the morning of the second day of the event, on 21 July 2016 and 27 July 2017, respectively. This phenomenon is known as an entrainment event and it has been observed previously in Granada (Bravo-Aranda et al., 2015). These figures suggest that these entrainments affect both the intensive and extensive aerosol properties.

The analyses of microphysical properties profiles show important differences in volume concentration between these two extreme events. For the DD event, coarse particles are predominant with VC_C between 200 and $300 \mu\text{m}^3 \text{cm}^{-3}$ on the aerosol layer, while for the BB event, the VC_C is very low ($\sim 10 \mu\text{m}^3 \text{cm}^{-3}$) and fine particles are predominant with maximum values between 60 and $105 \mu\text{m}^3 \text{cm}^{-3}$. In general, GRASP VC_F overestimates the SNS measurements with differences below $10 \mu\text{m}^3 \text{cm}^{-3}$, whereas GRASP VC_C is similar to the SNS measurements for values around $55 \mu\text{m}^3 \text{cm}^{-3}$ as shown in Sect. 4.1.1. However, for higher values of VC_C , GRASP overestimates the SNS data with differences between 10 and $20 \mu\text{m}^3 \text{cm}^{-3}$ as shown in Benavent et al. (2019).

For extensive optical properties, the σ_{sca} profiles at 532 nm show similar values between both events, with values between 200 and 400Mm^{-1} . However, for σ_{abs} there are significant differences between both events, with larger values observed during the BB event probably because of the presence of organic and black carbon particles. Nevertheless, we remark that σ_{abs} is not negligible as expected for mineral dust particles (e.g. Valenzuela et al., 2012). These findings are supported by SSA profiles that show lower SSA values for biomass burning (mean values ~ 0.83) and higher values for dust events (mean values ~ 0.93).

Finally, Figs. 9 and 10 also show the profiles obtained for intensive properties such as SAE and AAE computed from the GRASP retrievals (spectral range 355–1064 nm). The analyses of these variables can provide an indication of aerosol types. On 20 and 21 July 2016, the SAE values lower than 0.5 corroborate the predominance of coarse particles for mineral dust particles (Bergstrom et al., 2007) and the AAE values, ranging from 1.5 to 2.1, suggest a mixture of mineral dust and absorbing particles of anthropogenic origin (e.g. Giles et al., 2011; Valenzuela et al., 2015). During the BB event, the SAE values are around 2, indicating a scattering dominated by sub-micron particles, and the AAE values

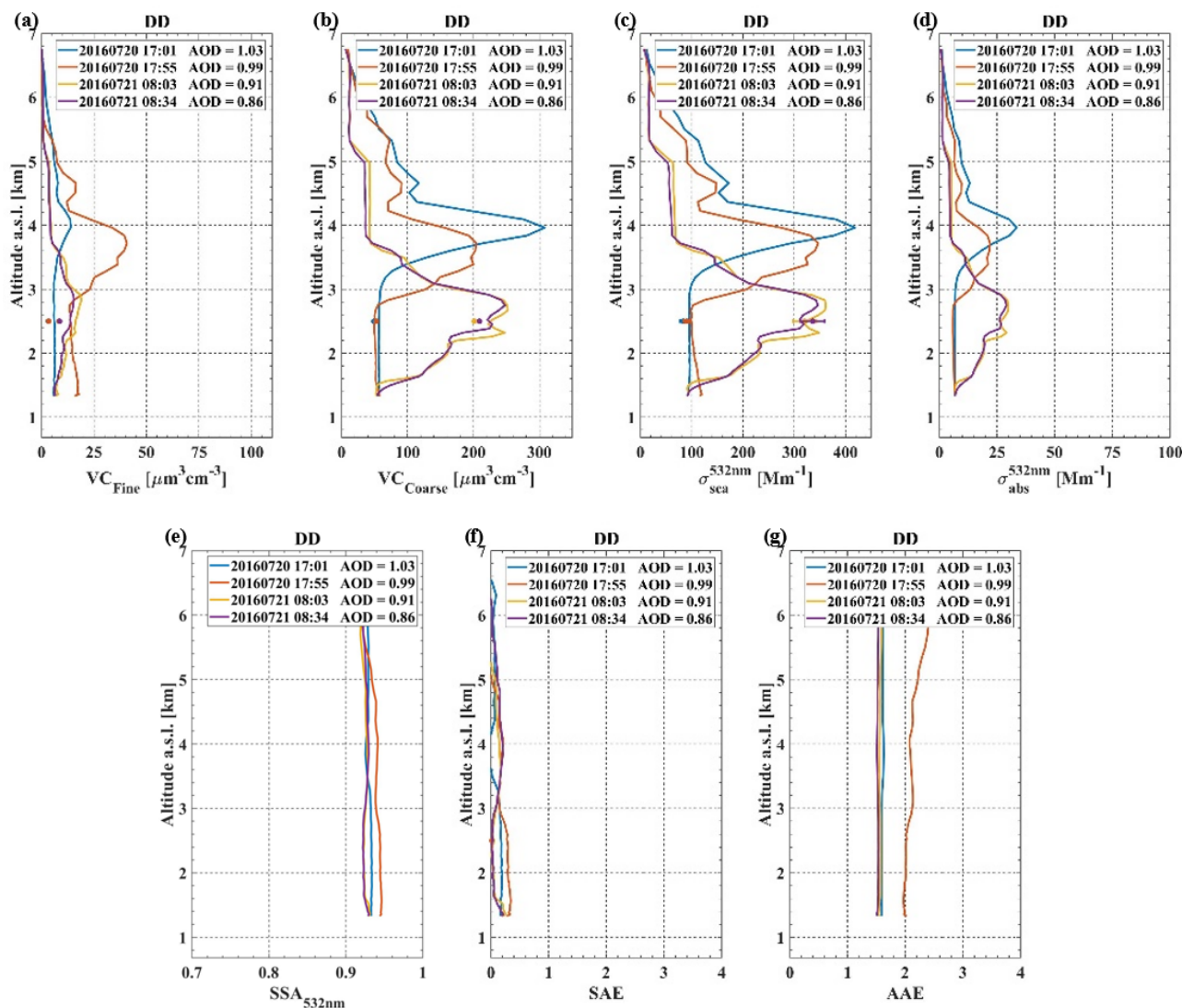


Figure 9. Volume concentration for (a) fine and (b) coarse modes, (c) scattering (σ_{sca}) and (d) absorption (σ_{abs}) coefficients, (e) single scattering albedo (SSA) at 532 nm, (f) scattering Ångström exponent (SAE), and (g) absorption Ångström exponent (AAE) retrieved by GRASP (line) and the SNS measurements (point) during the desert dust event on 20 and 21 July 2016. The AOD shown is at 440 nm.

between 1.1 and 1.45 suggest the presence of carbonaceous particles (Giles et al., 2012). Nevertheless, further advancement in the interpretation of aerosol chemical composition is currently challenging; however, new developments aimed at the characterization of aerosol compositions are being added to GRASP (Li et al., 2019, 2020) and will be explored in the future.

5 Conclusions

In this study, we presented an overview of aerosol optical and microphysical properties retrieved with the GRASP code during the SLOPE I and II field campaigns. The measurements from lidar and sun–sky photometer performed on May,

June, and July 2016 and 2017 were used as input data in GRASP to retrieve these aerosol properties.

The in situ measurements performed at the Sierra Nevada Station during the SLOPE I and II campaigns and the airborne measurement gathered during special periods on both campaigns allowed for the assessment of the aerosol properties retrieved by the GRASP code at 2.5 km a.s.l. and for the whole profile, respectively. The volume concentration comparison shows better agreement for the coarse mode ($R = 0.83$) than for the fine and total modes. The range of values for the fine mode is small due to the few cases (15 % of cases) with predominant fine particles; therefore, we cannot conclude that there is agreement between the GRASP retrievals and in situ measurements for the fine mode. For the scattering and absorption coefficients, the differences between

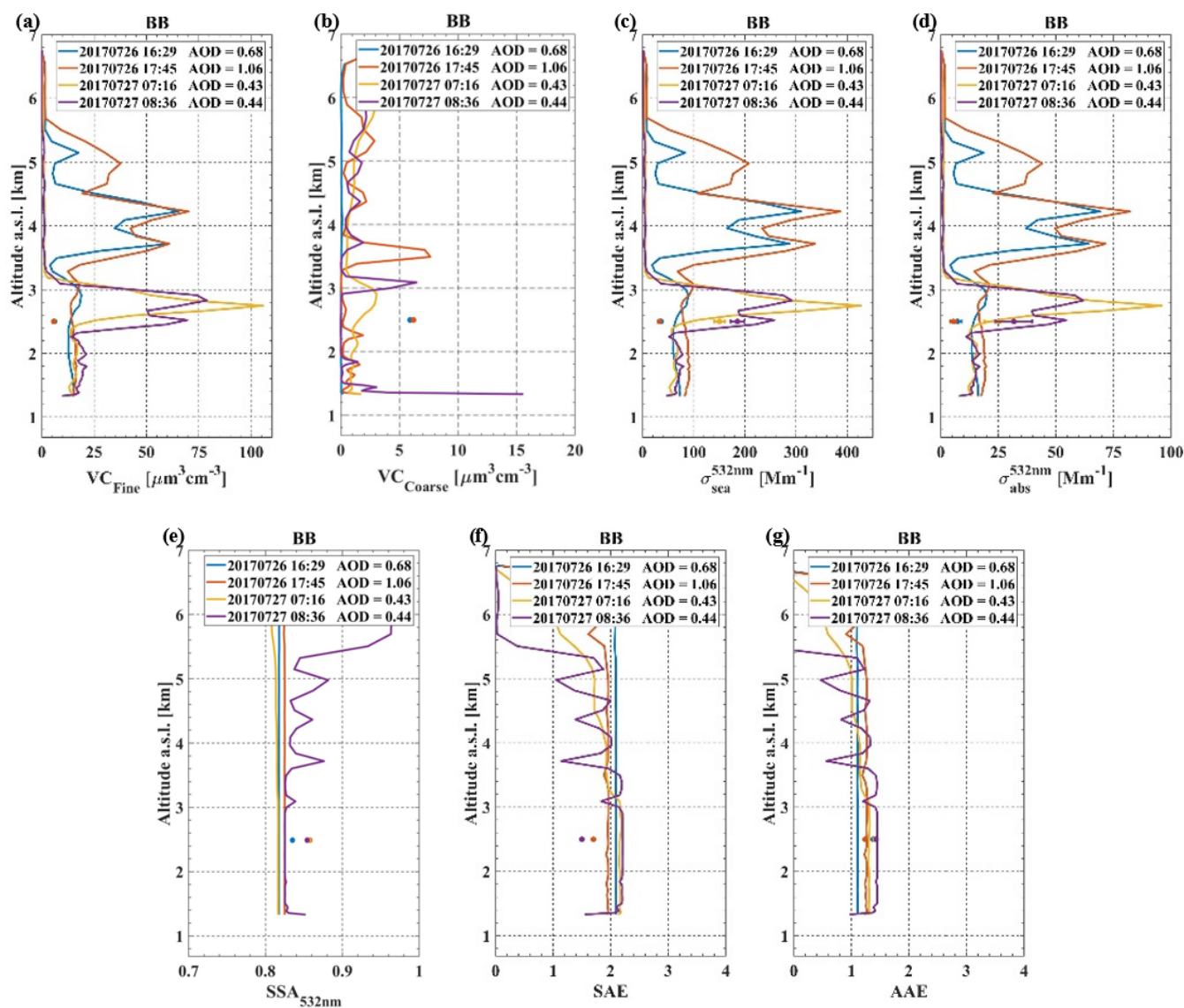


Figure 10. Volume concentration for (a) fine and (b) coarse modes, (c) scattering (σ_{sca}) and (d) absorption (σ_{abs}) coefficients, (e) single scattering albedo (SSA) at 532 nm, (f) scattering Ångström exponent (SAE), and (g) absorption Ångström exponent (AAE) retrieved by GRASP (line) and the SNS measurements (point) during biomass burning event on 26 and 27 July 2017. The AOD shown is at 440 nm.

the GRASP data at 2.5 km a.s.l. and in situ measurements are lowest for the longest wavelengths, with differences of $11 \pm 17 \text{ Mm}^{-1}$ at 450 nm and $2 \pm 6 \text{ Mm}^{-1}$ at 370 nm for σ_{sca} and σ_{abs} , respectively. The agreement between GRASP and in situ measurements at the SNS is solid for both scattering and absorption coefficients. In general, GRASP somewhat overestimates the in situ data at 2.5 km a.s.l. These differences (14 ± 10 and $1.2 \pm 1.2 \text{ Mm}^{-1}$ for σ_{sca} and σ_{abs} , respectively) are also observed in the whole profile when comparing the GRASP retrievals and the airborne measurements performed on 15, 17, and 18 June 2016 and 21, 23, and 24 June 2017.

The statistical analysis of the SLOPE I and II campaigns shows the values of aerosol optical depth

($\text{AOD}_{440} = 0.22 \pm 0.18$) and Ångström exponent ($\text{AE}_{440-870} = 0.8 \pm 0.4$) that are typical of those months in Granada. The large variety of aerosol properties values denotes a large variability of aerosol loads and types with a desert mineral dust predominance associated with North African intrusions in the south-east of Spain. The statistical overview of the volume concentration profiles shows a decay of the properties with altitude, reaching approximately zero at 4–5 km a.s.l. The coarse mode shows the highest variability with the 90th percentile values being between 40 and $60 \mu\text{m}^3 \text{cm}^{-3}$. The largest value for the absorption coefficient is observed at the lowest altitudes (4 Mm^{-1}). Finally, two extreme events ($\text{AOD}_{440} > 1.0$) were studied: a Saharan dust intrusion and biomass burning from fires

in Portugal in July 2016 and 2017, respectively. The study of these events shows the high capabilities of GRASP to retrieve volume concentration profiles in both fine and coarse mode and the potentially interesting capability of the algorithm to derive the profiles of the single scattering albedo and absorption coefficients for different types and sizes of atmospheric aerosols.

Data availability. The GRASP inversion algorithm software used in this work is free and publicly available at <http://www.grasp-open.com> (last access: 1 April 2020). Lidar and in situ data are available from the authors upon request. Sun–sky photometer data are accessible on the AERONET website (<http://aeronet.gsfc.nasa.gov/>, last access: 1 April 2020).

Author contributions. The conceptualization was done by JABO and LAA. JABO performed the GRASP retrievals, analysed the data, and wrote the manuscript. RR helped perform the GRASP retrievals. JACV and HL operated and processed the in situ measurement at the Sierra Nevada Station. GT, NP, and AA performed the installation of the instrumentation on board the aircraft and operated the instruments during the flights. AC processed the airborne in situ data. The lidar data acquisition was performed by JABO, GdAM, JLGR, POA, RR, and AEBV. MH and OD provided feedback on the GRASP algorithm. The formal analysis, investigation, writing of the original draft, preparation, review of the writing, and editing were performed by JABO, JACV, RR, DPR, HL, and MJGM. The project administration, funding acquisition, and design of the SLOPE I and II campaigns were done by FJOR and LAA. Coordination of the campaign was the responsibility of LAA. All authors provided comments on the manuscript and helped with manuscript corrections.

Competing interests. The authors declare that they have no conflict of interest.

Acknowledgements. Jose Antonio Benavent-Oltra is funded by the University of Granada through “Plan Propio. Programa 7, Convocatoria 2019”. Roberto Román is funded by MINECO under the post-doctoral programme Juan de la Cierva-Incorporación (IJCI2016-30007). Juan Andrés Casquero-Vera is funded by MINECO under the predoctoral programme FPI (BES-2017-080015). Maria J. Granados-Muñoz received funding from the European Union’s Horizon 2020 research and innovation programme under the Marie Skłodowska-Curie grant agreement No 796539. Oleg Dubovik was supported by the Labex CaPPA project, which is funded by the French National Research Agency under contract “ANR-11-LABX0005-01”. This work was also supported by the Spanish Ministry of Economy and Competitiveness (projects CMT2015-66742-R, CGL2016-81092-R, CGL2017-85344-R, RTI2018-097864-B-I00 and CGL2017-90884-REDT), by the Andalusia Regional Government through project P18-RT-3820 and the Unity of Excellence “María de Maeztu” (project MDM-2016-0600) financed by the Spanish State Research Agency (AEI). The authors thankfully ac-

knowledge the FEDER programme for the instrumentation used in this work, the University of Granada, which supported this study through the Excellence Units Program, and the Sierra Nevada National Park. We also thank Dr. Grisa Monick who provided the Aethalometer AVIO AE-33 installed on the aircraft. Thanks to AERONET and ACTRIS/AERONET Europe for the scientific and technical support. Finally, the authors would like to acknowledge the use of the GRASP inversion algorithm software (<http://www.grasp-open.com>, last access: 1 April 2020), in this work.

Financial support. This article is based upon work from COST Action CA18235 PROBE (PROfiling the atmospheric Boundary layer at European scale) and supported by COST (European Cooperation in Science and Technology; <http://www.cost.eu>, last access: 25 May 2021). This study was also supported by the Marie Skłodowska-Curie Research Innovation and Staff Exchange (RISE) GRASP-ACE (grant no. 778349) project.

Review statement. This paper was edited by Matthias Tesche and reviewed by three anonymous referees.

References

- Alados-Arboledas, L., Muller, D., Guerrero-Rascado, J. L., Navas-Guzman, F., Pérez-Ramírez, D., and Olmo, F. J.: Optical and microphysical properties of fresh biomass burning aerosol retrieved by Raman lidar, and star-and sun-photometry, *Geophys. Res. Lett.*, 38, L01807, <https://doi.org/10.1029/2010GL045999>, 2011.
- Amiridis, V., Balis, D. S., Kazadzis, S., Bais, A., Gianakaki, E., Papayannis, A., and Zerefos, C.: Four-year aerosol observations with a Raman lidar at Thessaloniki, Greece, in the framework of European Aerosol Research Lidar Network (EARLINET), *J. Geophys. Res.*, 110, D21203, <https://doi.org/10.1029/2005JD006190>, 2005.
- Anderson, T. L. and Ogren, J. A.: Determining aerosol radiative properties using the TSI 3563 integrating nephelometer, *Aerosol Sci. Technol.*, 29, 57–69, 1998.
- Ansmann, A., Riebesell, M., Wandinger, U., Weitkamp, C., Voss, E., Lahmann, W., and Michaelis, W.: Combined Raman elastic backscatter LIDAR vertical profiling of moisture, aerosol extinction, backscatter and LIDAR ratio, *Appl. Phys. B*, 55, 18–28, 1992.
- Barreto, Á., Cuevas, E., Granados-Muñoz, M. J., Alados-Arboledas, L., Romero, P. M., Gröbner, J., Kouremeti, N., Almansa, A. F., Stone, T., Toledano, C., Román, R., Sorokin, M., Holben, B., Canini, M., and Yela, M.: The new sun-sky-lunar Cimel CE318-T multiband photometer – a comprehensive performance evaluation, *Atmos. Meas. Tech.*, 9, 631–654, <https://doi.org/10.5194/amt-9-631-2016>, 2016.
- Barreto, Á., Román, R., Cuevas, E., Pérez-Ramírez, D., J. Berjón, A., Kouremeti, N., Kazadzis, S., Gröbner, J., Mazzola, M., Toledano, C., Benavent-Oltra, J. A., Doppler, L., Juryšek, J., Almansa, A. F., Victori, S., Maupin, F., Guirado-Fuentes, C., González, R., Vitale, V., Goloub, P., Blarel, L., Alados-Arboledas, L., Woolliams, E., Greenwell,

- C., Taylor, S., Antuña, J. C., and Yela, M.: Evaluation of night-time aerosols measurements and lunar irradiance models in the frame of the first multi-instrument nocturnal intercomparison campaign, *Atmos. Environ.*, 202, 190–211, <https://doi.org/10.1016/j.atmosenv.2019.01.006>, 2019.
- Bedoya-Velásquez, A. E., Navas-Guzmán, F., Granados-Muñoz, M. J., Titos, G., Román, R., Casquero-Vera, J. A., Ortiz-Amezcuca, P., Benavent-Oltra, J. A., de Arruda Moreira, G., Montilla-Rosero, E., Hoyos, C. D., Artiñano, B., Coz, E., Olmo-Reyes, F. J., Alados-Arboledas, L., and Guerrero-Rascado, J. L.: Hygroscopic growth study in the framework of EARLINET during the SLOPE I campaign: synergy of remote sensing and in situ instrumentation, *Atmos. Chem. Phys.*, 18, 7001–7017, <https://doi.org/10.5194/acp-18-7001-2018>, 2018.
- Bedoya-Velásquez, A. E., Navas-Guzmán, F., de Arruda Moreira, G., Román, R., Cazorla, A., Ortiz-Amezcuca, P., Benavent-Oltra, J. A., Alados-Arboledas, L., Olmo-Reyes, F. J., Foyo-Moreno, I., Montilla-Rosero, E., Hoyos, C. D., and Guerrero-Rascado, J. L.: Seasonal analysis of the atmosphere during five years by using microwave radiometry over a mid-latitude site, *Atmos. Res.*, 218, 78–89, <https://doi.org/10.1016/j.atmosres.2018.11.014>, 2019.
- Benavent-Oltra, J. A., Román, R., Granados-Muñoz, M. J., Pérez-Ramírez, D., Ortiz-Amezcuca, P., Denjean, C., Lopatin, A., Lyamani, H., Torres, B., Guerrero-Rascado, J. L., Fuertes, D., Dubovik, O., Chaikovsky, A., Olmo, F. J., Mallet, M., and Alados-Arboledas, L.: Comparative assessment of GRASP algorithm for a dust event over Granada (Spain) during ChArMEX-ADRIMED 2013 campaign, *Atmos. Meas. Tech.*, 10, 4439–4457, <https://doi.org/10.5194/amt-10-4439-2017>, 2017.
- Benavent-Oltra, J. A., Román, R., Casquero-Vera, J. A., Pérez-Ramírez, D., Lyamani, H., Ortiz-Amezcuca, P., Bedoya-Velásquez, A. E., de Arruda Moreira, G., Barreto, Á., Lopatin, A., Fuertes, D., Herrera, M., Torres, B., Dubovik, O., Guerrero-Rascado, J. L., Goloub, P., Olmo-Reyes, F. J., and Alados-Arboledas, L.: Different strategies to retrieve aerosol properties at night-time with the GRASP algorithm, *Atmos. Chem. Phys.*, 19, 14149–14171, <https://doi.org/10.5194/acp-19-14149-2019>, 2019.
- Bergstrom, R. W., Pilewskie, P., Russell, P. B., Redemann, J., Bond, T. C., Quinn, P. K., and Sierau, B.: Spectral absorption properties of atmospheric aerosols, *Atmos. Chem. Phys.*, 7, 5937–5943, <https://doi.org/10.5194/acp-7-5937-2007>, 2007.
- Böckmann, C.: Hybrid regularization method for the ill-posed inversion of multiwavelength lidar data to determine aerosol size distributions, *Appl. Optics*, 40, 1329–1342, 2001.
- Bravo-Aranda, J. A., Titos, G., Granados-Muñoz, M. J., Guerrero-Rascado, J. L., Navas-Guzmán, F., Valenzuela, A., Lyamani, H., Olmo, F. J., Andrey, J., and Alados-Arboledas, L.: Study of mineral dust entrainment in the planetary boundary layer by lidar depolarisation technique, *Tellus B*, 67, 26180, <https://doi.org/10.3402/tellusb.v67.26180>, 2015.
- Cariñanos, P., Foyo-Moreno, I., Alados, I., Guerrero-Rascado, J. L., Ruiz-Peñuela, S., Titos, G., Cazorla, A., Alados-Arboledas, L., and Díaz de la Guardia, C.: Bioaerosols in urban environments: Trends and interactions with pollutants and meteorological variables based on quasi-climatological series, *J. Environ. Manage.*, 282, 111963, <https://doi.org/10.1016/j.jenvman.2021.111963>, 2021.
- Casquero-Vera, J. A., Lyamani, H., Dada, L., Hakala, S., Paasonen, P., Román, R., Fraile, R., Petäjä, T., Olmo-Reyes, F. J., and Alados-Arboledas, L.: New particle formation at urban and high-altitude remote sites in the south-eastern Iberian Peninsula, *Atmos. Chem. Phys.*, 20, 14253–14271, <https://doi.org/10.5194/acp-20-14253-2020>, 2020.
- Casquero-Vera, J. A., Lyamani, H., Titos, G., Minguillón, M. C., Dada, L., Alastuey, A., Querol X., Petäjä T., Olmo F. J., and Alados-Arboledas L.: Quantifying traffic, biomass burning and secondary source contributions to atmospheric particle number concentrations at urban and suburban sites, *Sci. Total Environ.*, 768, 145282, <https://doi.org/10.1016/j.scitotenv.2021.145282>, 2021.
- Cazorla, A., Bahadur, R., Suski, K. J., Cahill, J. F., Chand, D., Schmid, B., Ramanathan, V., and Prather, K. A.: Relating aerosol absorption due to soot, organic carbon, and dust to emission sources determined from in-situ chemical measurements, *Atmos. Chem. Phys.*, 13, 9337–9350, <https://doi.org/10.5194/acp-13-9337-2013>, 2013.
- Caumont, O., Cimini, D., Löhnert, U., Alados-Arboledas, L., Bleisch, R., Buffa, F., Ferrario, M. E., Haeefe, A., Huet, T., Madonna, F., and Pace, G.: Assimilation of humidity and temperature observations retrieved from ground-based microwave radiometers into a convective-scale NWP model, *Q. J. Roy. Meteorol. Soc.*, 142, 2692–2704, <https://doi.org/10.1002/qj.2860>, 2016.
- Chaikovsky, A., Dubovik, O., Holben, B., Bril, A., Goloub, P., Tanré, D., Pappalardo, G., Wandinger, U., Chaikovskaya, L., Denisov, S., Grudo, J., Lopatin, A., Karol, Y., Lapyonok, T., Amiridis, V., Ansmann, A., Apituley, A., Alados-Arboledas, L., Binietoglou, I., Boselli, A., D'Amico, G., Freudenthaler, V., Giles, D., Granados-Muñoz, M. J., Kokkalis, P., Nicolae, D., Oschepkov, S., Papayannis, A., Perrone, M. R., Pietruczuk, A., Roca-denbosch, F., Sicard, M., Slutsker, I., Talianu, C., De Tomasi, F., Tsekeri, A., Wagner, J., and Wang, X.: Lidar-Radiometer Inversion Code (LIRIC) for the retrieval of vertical aerosol properties from combined lidar/radiometer data: development and distribution in EARLINET, *Atmos. Meas. Tech.*, 9, 1181–1205, <https://doi.org/10.5194/amt-9-1181-2016>, 2016.
- Chen, C., Dubovik, O., Henze, D. K., Lapyonok, T., Chin, M., Ducos, F., Litvinov, P., Huang, X., and Li, L.: Retrieval of desert dust and carbonaceous aerosol emissions over Africa from POLDER/PARASOL products generated by the GRASP algorithm, *Atmos. Chem. Phys.*, 18, 12551–12580, <https://doi.org/10.5194/acp-18-12551-2018>, 2018.
- Chen, C., Dubovik, O., Henze, D. K., Chin, M., Lapyonok, T., Schuster, G. L., Ducos, F., Fuertes, D., Litvinov, P., Li, L., Lopatin, A., Hu, Q., and Torres, B.: Constraining global aerosol emissions using POLDER/PARASOL satellite remote sensing observations, *Atmos. Chem. Phys.*, 19, 14585–14606, <https://doi.org/10.5194/acp-19-14585-2019>, 2019.
- de Arruda Moreira, G., Guerrero-Rascado, J. L., Bravo-Aranda, J. A., Benavent-Oltra, J. A., Ortiz-Amezcuca, P., Román, R., Bedoya-Velásquez, A. E., Landulfo, E., and Alados-Arboledas, L.: Study of the planetary boundary layer by microwave radiometer, elastic lidar and Doppler lidar estimations in Southern Iberian Peninsula, *Atmos. Res.*, 213, 185–195, <https://doi.org/10.1016/j.atmosres.2018.06.007>, 2018.

- de Arruda Moreira, G., Guerrero-Rascado, J. L., Benavent-Oltra, J. A., Ortiz-Amezcuca, P., Román, R., E. Bedoya-Velásquez, A., Bravo-Aranda, J. A., Olmo Reyes, F. J., Landulfo, E., and Alados-Arboledas, L.: Analyzing the turbulent planetary boundary layer by remote sensing systems: the Doppler wind lidar, aerosol elastic lidar and microwave radiometer, *Atmos. Chem. Phys.*, 19, 1263–1280, <https://doi.org/10.5194/acp-19-1263-2019>, 2019.
- del Águila, A., Sorribas, M., Lyamani, H., Titos, G., Olmo, F. J., Arruda-Moreira, G., Yela, M., and Alados-Arboledas, L.: Sources and physicochemical characteristics of submicron aerosols during three intensive campaigns in Granada (Spain), *Atmos. Res.*, 213, 398–410, <https://doi.org/10.1016/j.atmosres.2018.06.004>, 2018.
- Dubovik, O. and King, M. D.: A flexible inversion algorithm for retrieval of aerosol optical properties from Sun and sky radiance measurements, *J. Geophys. Res.*, 105, 20673–20696, 2000.
- Dubovik, O., Smirnov, A., Holben, B. N., King, M. D., Kaufman, Y., Eck, T. F., and Slutsker, I.: Accuracy assessments of aerosol optical properties retrieved from Aerosol Robotic Network (AERONET) Sun and sky radiance measurements, *J. Geophys. Res.*, 105, 9791–9806, 2000.
- Dubovik, O., Herman, M., Holdak, A., Lapyonok, T., Tanré, D., Deuzé, J. L., Ducos, F., Sinyuk, A., and Lopatin, A.: Statistically optimized inversion algorithm for enhanced retrieval of aerosol properties from spectral multi-angle polarimetric satellite observations, *Atmos. Meas. Tech.*, 4, 975–1018, <https://doi.org/10.5194/amt-4-975-2011>, 2011.
- Dubovik, O., Lapyonok, T., Litvinov, P., Herman, M., Fuertes, D., Ducos, F., Lopatin, A., Chaikovskiy, A., Torres, B., Derimian, Y., Huang, X., Lopatin, A., Chaikovskiy, A., Aspetsberger, M., and Federspiel, C.: Grasp: a versatile algorithm for characterizing the atmosphere, *SPIE Newsroom*, 25, <https://doi.org/10.1117/2.1201408.005558>, 2014.
- Dubovik, O., Li, Z., Mishchenko, M. I., Tanré, D., Karol, Y., Bojkov, B., Cairns, B., Diner, D. J., Espinosa, W. R., Goloub, P., Gu, X., Hasekamp, O., Hong, J., Hou, W., Knobelspiess, K. D., Landgraf, J., Li, L., Litvinov, P., Liu, Y., Lopatin, A., Marbach, T., Maring, H., Martins, V., Meijer, Y., Milinevsky, G., Mukai, S., Parol, F., Qiao, Y., Remer, L., Rietjens, J., Sano, I., Stammes, P., Stammes, S., Sun, X., Tabary, P., Travis, L. D., Waquet, F., Xu, F., Yan, C., and Yin, D.: Polarimetric remote sensing of atmospheric aerosols: Instruments, methodologies, results, and perspectives, *J. Q. Spectrosc. Ra.*, 224, 474–511, <https://doi.org/10.1016/j.jqsrt.2018.11.024>, 2019.
- Drinovec, L., Močnik, G., Zotter, P., Prévôt, A. S. H., Ruckstuhl, C., Coz, E., Rupakheti, M., Sciare, J., Müller, T., Wiedensohler, A., and Hansen, A. D. A.: The “dual-spot” Aethalometer: an improved measurement of aerosol black carbon with real-time loading compensation, *Atmos. Meas. Tech.*, 8, 1965–1979, <https://doi.org/10.5194/amt-8-1965-2015>, 2015.
- Espinosa, W. R., Remer, L. A., Dubovik, O., Ziemba, L., Beyersdorf, A., Orozco, D., Schuster, G., Lapyonok, T., Fuertes, D., and Martins, J. V.: Retrievals of aerosol optical and microphysical properties from Imaging Polar Nephelometer scattering measurements, *Atmos. Meas. Tech.*, 10, 811–824, <https://doi.org/10.5194/amt-10-811-2017>, 2017.
- Fernald, F. G.: Analysis of atmospheric lidar observations- Some comments, *App. Optics*, 23, 652–653, 1984.
- Fernald, F. G., Herman, B. M., and Reagan, J. A.: Determination of aerosol height distributions by lidar, *J. Appl. Meteorol.*, 11, 482–489, 1972.
- Giles, D. M., Holben, B. N., Tripathi, S. N., Eck, T. F., Newcomb, W. W., Slutsker, I., Dickerson, R. R., Thompson, A. M., Mattoo, S., Wang, S., Singh, R. P., Sinyuk, A., and Schafer, J. S.: Aerosol properties over the Indo-Gangetic Plain: A mesoscale perspective from the TIGERZ experiment, *J. Geophys. Res.-Atmos.*, 116, D18203, <https://doi.org/10.1029/2011JD015809>, 2011.
- Giles, D. M., Holben, B. N., Eck, T. F., Sinyuk, A., Smirnov, A., Slutsker, I., Dickerson, R. R., Thompson, A. M., and Schafer, J. S.: An analysis of AERONET aerosol absorption properties and classifications representative of aerosol source regions, *J. Geophys. Res.-Atmos.*, 117, 127–135, <https://doi.org/10.1029/2012JD018127>, 2012.
- Giles, D. M., Sinyuk, A., Sorokin, M. G., Schafer, J. S., Smirnov, A., Slutsker, I., Eck, T. F., Holben, B. N., Lewis, J. R., Campbell, J. R., Welton, E. J., Korkin, S. V., and Lyapustin, A. I.: Advancements in the Aerosol Robotic Network (AERONET) Version 3 database – automated near-real-time quality control algorithm with improved cloud screening for Sun photometer aerosol optical depth (AOD) measurements, *Atmos. Meas. Tech.*, 12, 169–209, <https://doi.org/10.5194/amt-12-169-2019>, 2019.
- Granados-Muñoz, M. J., Sicard, M., Román, R., Benavent-Oltra, J. A., Barragán, R., Brogniez, G., Denjean, C., Mallet, M., Formenti, P., Torres, B., and Alados-Arboledas, L.: Impact of mineral dust on shortwave and longwave radiation: evaluation of different vertically resolved parameterizations in 1-D radiative transfer computations, *Atmos. Chem. Phys.*, 19, 523–542, <https://doi.org/10.5194/acp-19-523-2019>, 2019.
- Granados-Muñoz, M. J., Benavent-Oltra, J. A., Pérez-Ramírez, D., Lyamani, H., Guerrero-Rascado, J. L., Bravo-Aranda, J. A., Navas-Guzmán, F., Valenzuela, A., Olmo, F. J., and Alados-Arboledas, L.: Evaluation of LIRIC algorithm performance using independent sun-sky photometer data at two altitude levels, *Remote Sens.*, 12, 842, <https://doi.org/10.3390/rs12050842>, 2020.
- Guerrero-Rascado, J. L., Ruiz, B., and Alados Arboledas, L.: Multispectral Lidar characterization of the vertical structure of Saharan dust aerosol over southern Spain, *Atmos. Environ.*, 42, 2668–2681, <https://doi.org/10.1016/j.atmosenv.2007.12.062>, 2008.
- Guerrero-Rascado, J. L., Olmo, F. J., Avilés-Rodríguez, I., Navas-Guzmán, F., Pérez-Ramírez, D., Lyamani, H., and Alados Arboledas, L.: Extreme Saharan dust event over the southern Iberian Peninsula in september 2007: active and passive remote sensing from surface and satellite, *Atmos. Chem. Phys.*, 9, 8453–8469, <https://doi.org/10.5194/acp-9-8453-2009>, 2009.
- Herreras, M., Román, R., Cazorla, A., Toledano, C., Lyamani, H., Torres, B., Cachorro, V.E., Olmo, F. J., Alados-Arboledas, L., and de Frutos, A. M.: Evaluation of retrieved aerosol extinction profiles using as reference the aerosol optical depth differences between various heights, *Atmos. Res.*, 230, 104625, <https://doi.org/10.1016/j.atmosres.2019.104625>, 2019.
- Holben, B. N., Eck, T. F., Slutsker, I., Tanre, D., Buis, J. P., Setzer, A., Vermote, E., Reagan, J. A., Kaufman, Y. J., Nakajima, T., Lavenu, F., Jankowiak, I., and Smirnov, A.: AERONET-a federated instrument network a data archive for aerosol characterization, *Remote Sens. Environ.*, 66, 1–16, 1998.
- Horvath, H., Alados Arboledas, L., and Olmo Reyes, F. J.: Angular scattering of the Sahara dust aerosol, *Atmos. Chem.*

- Phys., 18, 17735–17744, <https://doi.org/10.5194/acp-18-17735-2018>, 2018.
- IPCC: Contribution of Working Group I to the Fifth Assessment Report of the Intergovernmental Panel on Climate Change, Summary for Policymakers in Climate Change, Stocker, Cambridge University Press, Cambridge, 2013.
- Klett, J. D.: Stable analytical inversion solution for processing lidar returns, *Appl. Optics*, 20, 211–220, 1981.
- Klett, J. D.: Lidar inversion with variable backscatter/extinction ratios, *Appl. Opt.*, 24, 1638–1643, 1985.
- Li, L., Dubovik, O., Derimian, Y., Schuster, G. L., Lapyonok, T., Litvinov, P., Ducos, F., Fuertes, D., Chen, C., Li, Z., Lopatin, A., Torres, B., and Che, H.: Retrieval of aerosol components directly from satellite and ground-based measurements, *Atmos. Chem. Phys.*, 19, 13409–13443, <https://doi.org/10.5194/acp-19-13409-2019>, 2019.
- Li, L., Che, H., Derimian, Y., Dubovik, O., Schuster, G., Chen, C., Lid, Q., Wang, Y., Guo, B., and Zhang, X.: Retrievals of fine mode light-absorbing carbonaceous aerosols from POLDER/PARASOL observations over East and South Asia, *Remote Sens. Environ.*, 247, 111913, <https://doi.org/10.1016/j.rse.2020.111913>, 2020.
- Liu, D., Taylor, J. W., Crosier, J., Marsden, N., Bower, K. N., Lloyd, G., Ryder, C. L., Brooke, J. K., Cotton, R., Marengo, F., Blyth, A., Cui, Z., Estelles, V., Gallagher, M., Coe, H., and Choulaton, T. W.: Aircraft and ground measurements of dust aerosols over the west African coast in summer 2015 during ICE-D and AER-D, *Atmos. Chem. Phys.*, 18, 3817–3838, <https://doi.org/10.5194/acp-18-3817-2018>, 2018.
- Lopatin, A., Dubovik, O., Chaikovskiy, A., Goloub, P., Lapyonok, T., Tanré, D., and Litvinov, P.: Enhancement of aerosol characterization using synergy of lidar and sun-photometer coincident observations: the GARRLiC algorithm, *Atmos. Meas. Tech.*, 6, 2065–2088, <https://doi.org/10.5194/amt-6-2065-2013>, 2013.
- Lyamani, H., Olmo, F. J., and Alados-Arboledas, L.: Physical and optical properties of aerosols over an urban location in Spain: seasonal and diurnal variability, *Atmos. Chem. Phys.*, 10, 239–254, <https://doi.org/10.5194/acp-10-239-2010>, 2010.
- Mallet, M., Dulac, F., Formenti, P., Nabat, P., Sciare, J., Roberts, G., Pelon, J., Ancellet, G., Tanré, D., Parol, F., Denjean, C., Brogniez, G., di Sarra, A., Alados-Arboledas, L., Arndt, J., Auriol, F., Blarel, L., Bourriane, T., Chazette, P., Chevaillier, S., Claeys, M., D’Anna, B., Derimian, Y., Desboeufs, K., Di Iorio, T., Doussin, J.-F., Durand, P., Féron, A., Freney, E., Gaimoz, C., Goloub, P., Gómez-Amo, J. L., Granados-Muñoz, M. J., Grand, N., Hamonou, E., Jankowiak, I., Jeannot, M., Léon, J.-F., Maillé, M., Mailler, S., Meloni, D., Menut, L., Momboisse, G., Nicolas, J., Podvin, T., Pont, V., Rea, G., Renard, J.-B., Roblou, L., Schepanski, K., Schwarzenboeck, A., Sellegri, K., Sicard, M., Solmon, F., Somot, S., Torres, B., Totems, J., Triquet, S., Verdier, N., Verwaerde, C., Waquet, F., Wenger, J., and Zapf, P.: Overview of the Chemistry-Aerosol Mediterranean Experiment/Aerosol Direct Radiative Forcing on the Mediterranean Climate (ChArMEx/ADRMED) summer 2013 campaign, *Atmos. Chem. Phys.*, 16, 455–504, <https://doi.org/10.5194/acp-16-455-2016>, 2016.
- Müller, D., Wandinger, U., and Ansmann, A.: Microphysical particle parameters from extinction and backscatter lidar data by inversion with regularization: simulation, *Appl. Opt.* 38, 2358–2368, 1999.
- Müller, D., Ansmann, A., Mattis, I., Tesche, M., Wandinger, U., Althausen, D., and Pisani, G.: Aerosol-type-dependent lidar ratios observed with Raman lidar, *J. Geophys. Res.-Atmos.*, 112, D16202, <https://doi.org/10.1029/2006jd008292>, 2007.
- Müller, T., Laborde, M., Kassell, G., and Wiedensohler, A.: Design and performance of a three-wavelength LED-based total scatter and backscatter integrating nephelometer, *Atmos. Meas. Tech.*, 4, 1291–1303, <https://doi.org/10.5194/amt-4-1291-2011>, 2011.
- Navas-Guzmán, F., Bravo-Aranda, J. A., Guerrero-Rascado, J. L., Granados-Muñoz, M. J., and Alados-Arboledas, L.: Statistical analysis of aerosol optical properties retrieved by Raman lidar over Southeastern Spain, *Tellus B*, 65, 21234, <https://doi.org/10.3402/tellusb.v65i0.21234>, 2013.
- Navas-Guzmán, F., Fernández-Gálvez, J., Granados-Muñoz, M. J., Guerrero-Rascado, J. L., Bravo-Aranda, J. A., and Alados-Arboledas, L.: Tropospheric water vapour and relative humidity profiles from lidar and microwave radiometry, *Atmos. Meas. Tech.*, 7, 1201–1211, <https://doi.org/10.5194/amt-7-1201-2014>, 2014.
- Ortiz-Amezcuca, P., Guerrero-Rascado, J. L., Granados-Muñoz, M. J., Benavent-Oltra, J. A., Böckmann, C., Samaras, S., Stachlewska, I. S., Janicka, E., Baars, H., Bohlmann, S., and Alados-Arboledas, L.: Microphysical characterization of long-range transported biomass burning particles from North America at three EARLINET stations, *Atmos. Chem. Phys.*, 17, 5931–5946, <https://doi.org/10.5194/acp-17-5931-2017>, 2017.
- Ortiz-Amezcuca, P., Bedoya-Velásquez, A. E., Benavent-Oltra, J. A., Pérez-Ramírez, D., Veselovskii, I., Castro-Santiago, M., Bravo-Aranda, J. A., Guedes, A., Guerrero-Rascado, J. L., and Alados-Arboledas, L.: Implementation of UV rotational Raman channel to improve aerosol retrievals from multiwavelength lidar, *Opt. Express*, 28, 8156–8168, <https://doi.org/10.1364/OE.383441>, 2020.
- Pappalardo, G., Amodeo, A., Apituley, A., Comeron, A., Freudenthaler, V., Linné, H., Ansmann, A., Bösenberg, J., D’Amico, G., Mattis, I., Mona, L., Wandinger, U., Amiridis, V., Alados-Arboledas, L., Nicolae, D., and Wiegner, M.: EARLINET: towards an advanced sustainable European aerosol lidar network, *Atmos. Meas. Tech.*, 7, 2389–2409, <https://doi.org/10.5194/amt-7-2389-2014>, 2014.
- Pérez-Ramírez, D., Lyamani, H., Olmo, F. J., Whiteman, D. N., and Alados-Arboledas, L.: Columnar aerosol properties from sun-and-star photometry: statistical comparisons and day-to-night dynamic, *Atmos. Chem. Phys.*, 12, 9719–9738, <https://doi.org/10.5194/acp-12-9719-2012>, 2012.
- Pérez-Ramírez, D., Lyamani, H., Smirnov, A., O’Neill, N. T., Veselovskii, I., Whiteman, D. N., Olmo, F. J., and Alados-Arboledas, L.: Statistical study of day and night hourly patterns of columnar aerosol properties using sun and star photometry, *Proc. SPIE*, 100001, <https://doi.org/10.1117/12.2242372>, 2016.
- Pérez-Ramírez, D., Whiteman, D. N., Veselovskii, I., Colarco, P., Korenski, M., and da Silva, A.: Retrievals of aerosol single scattering albedo by multiwavelength lidar measurements: Evaluations with NASA Langley HSRL-2 during discover-AQ field campaigns, *Remote Sens. Environ.*, 222, 144–164, 2019.
- Román, R., Cazorla, A., Toledano, C., Olmo, F. J., Cachorro, V. E., de Frutos, A., and Alados-Arboledas, L.: Cloud

- cover detection combining high dynamic range sky images and ceilometer measurements, *Atmos. Res.*, 196, 224–236, <https://doi.org/10.1016/j.atmosres.2017.06.006>, 2017.
- Román, R., Benavent-Oltra, J. A., Casquero-Vera, J. A., Lopatin, A., Cazorla, A., Lyamani, H., Denjean, C., Fuertes, D., Pérez-Ramírez, D., Torres, B., Toledano, C., Dubovik, O., Cachorro, V. E., de Frutos, Á., Olmo, F. J., and Alados-Arboledas, L.: Retrieval of aerosol profiles combining sun photometer and ceilometer measurements in GRASP code, *Atmos. Res.*, 204, 161–177, <https://doi.org/10.1016/j.atmosres.2018.01.021>, 2018.
- Román, R., González, R., Toledano, C., Barreto, Á., Pérez-Ramírez, D., Benavent-Oltra, J. A., Olmo, F. J., Cachorro, V. E., Alados-Arboledas, L., and de Frutos, Á. M.: Correction of a lunar-irradiance model for aerosol optical depth retrieval and comparison with a star photometer, *Atmos. Meas. Tech.*, 13, 6293–6310, <https://doi.org/10.5194/amt-13-6293-2020>, 2020.
- Rose, T., Crewell, S., Löhnert, U., and Simmer, C.: A network suitable microwave radiometer for operational monitoring of the cloudy atmosphere, *Atmos. Res.*, 75, 183–200, 2005.
- Russell, P. B., Bergstrom, R. W., Shinozuka, Y., Clarke, A. D., DeCarlo, P. F., Jimenez, J. L., Livingston, J. M., Redemann, J., Dubovik, O., and Strawa, A.: Absorption Angstrom Exponent in AERONET and related data as an indicator of aerosol composition, *Atmos. Chem. Phys.*, 10, 1155–1169, <https://doi.org/10.5194/acp-10-1155-2010>, 2010.
- Shin, S.-K., Tesche, M., Kim, K., Kezoudi, M., Tatarov, B., Müller, D., and Noh, Y.: On the spectral depolarisation and lidar ratio of mineral dust provided in the AERONET version 3 inversion product, *Atmos. Chem. Phys.*, 18, 12735–12746, <https://doi.org/10.5194/acp-18-12735-2018>, 2018.
- Sicard, M., Granados-Muñoz, M. J., Alados-Arboledas, L., Baragán, R., Bedoya-Velásquez, A.E., Benavent-Oltra, J. A., Bortoli, D., Comerón, A., Córdoba-Jabonero, C., Costa, M. J., del Águila, A., Fernández, A. J., Guerrero-Rascado, J. L., Jorba, O., Molero, F., Muñoz-Porcar, C., Ortiz-Amezcuca, P., Papa- giannopoulos, N., Potes, M., Pujadas, M., Rocadenbosch, F., Rodríguez-Gómez, A., Román, R., Salgado, R., Salgueiro, V., Sola, Y., and Yela, M.: Ground/space, passive/active remote sensing observations coupled with particle dispersion modelling to understand the inter-continental transport of wildfire smoke plumes, *Remote Sens. Environ.*, 232, 111294, <https://doi.org/10.1016/j.rse.2019.111294>, 2019.
- Sinyuk, A., Holben, B. N., Eck, T. F., Giles, D. M., Slutsker, I., Korkin, S., Schafer, J. S., Smirnov, A., Sorokin, M., and Lyapustin, A.: The AERONET Version 3 aerosol retrieval algorithm, associated uncertainties and comparisons to Version 2, *Atmos. Meas. Tech.*, 13, 3375–3411, <https://doi.org/10.5194/amt-13-3375-2020>, 2020.
- Sorribas, M., Olmo, F. J., Quirantes, A., Lyamani, H., Gil-Ojeda, M., Alados-Arboledas, L., and Horvath, H.: Role of spheroidal particles in closure studies for aerosol microphysical-optical properties, *Q. J. Roy. Meteorol. Soc.*, 141, 2700–2707, 2015.
- Tanré, D., Haywood, J., Pelon, J., Léon, J. F., Chatenet, B., Formenti, P., Francis, P., Goloub, P., Highwood, E. J., and Myhre, G.: Measurements and modeling of the Saharan dust radiative impact: overview of the Saharan Dust Experiment (SHADE), *J. Geophys. Res.*, 108, 18, <https://doi.org/10.1029/2002JD003273>, 2003.
- Titos, G., Ealo, M., Román, R., Cazorla, A., Sola, Y., Dubovik, O., Alastuey, A., and Pandolfi, M.: Retrieval of aerosol properties from ceilometer and photometer measurements: long-term evaluation with in situ data and statistical analysis at Montsec (southern Pyrenees), *Atmos. Meas. Tech.*, 12, 3255–3267, <https://doi.org/10.5194/amt-12-3255-2019>, 2019.
- Torres, B., Dubovik, O., Fuertes, D., Schuster, G., Cachorro, V. E., Lapyonok, T., Goloub, P., Blarel, L., Barreto, A., Mallet, M., Toledano, C., and Tanré, D.: Advanced characterisation of aerosol size properties from measurements of spectral optical depth using the GRASP algorithm, *Atmos. Meas. Tech.*, 10, 3743–3781, <https://doi.org/10.5194/amt-10-3743-2017>, 2017.
- Tsekeri, A., Lopatin, A., Amiridis, V., Marinou, E., Igloffstein, J., Siomos, N., Solomos, S., Kokkalis, P., Engelmann, R., Baars, H., Gratesea, M., Raptis, P. I., Biniotoglou, I., Mihalopoulos, N., Kalivitis, N., Kouvarakis, G., Bartsotas, N., Kallos, G., Basart, S., Schuettmeyer, D., Wandinger, U., Ansmann, A., Chaikovskiy, A. P., and Dubovik, O.: GARRLiC and LIRIC: strengths and limitations for the characterization of dust and marine particles along with their mixtures, *Atmos. Meas. Tech.*, 10, 4995–5016, <https://doi.org/10.5194/amt-10-4995-2017>, 2017.
- Turco, M., Jerez, S., Augusto, S., Tarín-Carrasco, P., Ratola, N., Jiménez-Guerrero, P., and Trigo, R. M.: Climate drivers of the 2017 devastating fires in Portugal, *Sci. Rep.*, 9, 13886, <https://doi.org/10.1038/s41598-019-50281-2>, 2019.
- Valenzuela, A., Olmo, F. J., Lyamani, H., Antón, M., Quirantes, A., Alados-Arboledas, L.: Analysis of the desert dust radiative properties over Granada using principal plane sky radiances and spheroids retrieval procedure, *Atmos. Res.*, 104/105, 292–301, <https://doi.org/10.1016/j.atmosres.2011.11.005>, 2012.
- Valenzuela, A., Olmo, F. J., Lyamani, H., Antón, M., Titos, G., Cazorla, A., and Alados-Arboledas, L.: Aerosol scattering and absorption Angström exponents as indicators of dust and dust-free days over Granada (Spain), *Atmos. Res.*, 154, 1–13, <https://doi.org/10.1016/j.atmosres.2014.10.015>, 2015.
- Vandenbussche, S., Callewaert, S., Schepanski, K., and De Mazière, M.: North African mineral dust sources: new insights from a combined analysis based on 3D dust aerosol distributions, surface winds and ancillary soil parameters, *Atmos. Chem. Phys.*, 20, 15127–15146, <https://doi.org/10.5194/acp-20-15127-2020>, 2020.
- Veselovskii, I., Kolgotin, A., Griaznov, V., Muller, D., Wandinger, U., and Whiteman, D.: Inversion with regularization for the retrieval of tropospheric aerosol parameters from multiwavelength lidar sounding, *Appl. Opt.*, 41, 3685–3699, 2002.
- Veselovskii, I., Whiteman, D. N., Korenskiy, M., Suvorina, A., and Pérez-Ramírez, D.: Use of rotational Raman measurements in multiwavelength aerosol lidar for evaluation of particle backscattering and extinction, *Atmos. Meas. Tech.*, 8, 4111–4122, <https://doi.org/10.5194/amt-8-4111-2015>, 2015.
- Veselovskii, I., Goloub, P., Podvin, T., Bovchaliuk, V., Derimian, Y., Augustin, P., Fourmentin, M., Tanre, D., Korenskiy, M., Whiteman, D. N., Diallo, A., Ndiaye, T., Kolgotin, A., and Dubovik, O.: Retrieval of optical and physical properties of African dust from multiwavelength Raman lidar measurements during the SHADOW campaign in Senegal, *Atmos. Chem. Phys.*, 16, 7013–7028, <https://doi.org/10.5194/acp-16-7013-2016>, 2016.

- Whiteman, D. N., Melfi, S. H., and Ferrare, R. A.: Raman lidar system for the measurement of water vapor and aerosols in the Earth's atmosphere, *Appl. Optics*, 31, 3068–3082, 1992.
- Wiedensohler, A., Birmili, W., Nowak, A., Sonntag, A., Weinhold, K., Merkel, M., Wehner, B., Tuch, T., Pfeifer, S., Fiebig, M., Fjåraa, A. M., Asmi, E., Sellegri, K., Depuy, R., Venzac, H., Villani, P., Laj, P., Aalto, P., Ogren, J. A., Swietlicki, E., Williams, P., Roldin, P., Quincey, P., Hüglin, C., Fierz-Schmidhauser, R., Gysel, M., Weingartner, E., Riccobono, F., Santos, S., Grünig, C., Faloon, K., Beddows, D., Harrison, R., Monahan, C., Jennings, S. G., O'Dowd, C. D., Marinoni, A., Horn, H.-G., Keck, L., Jiang, J., Scheckman, J., McMurry, P. H., Deng, Z., Zhao, C. S., Moerman, M., Henzing, B., de Leeuw, G., Löschau, G., and Bastian, S.: Mobility particle size spectrometers: harmonization of technical standards and data structure to facilitate high quality long-term observations of atmospheric particle number size distributions, *Atmos. Meas. Tech.*, 5, 657–685, <https://doi.org/10.5194/amt-5-657-2012>, 2012.
- Wiedensohler, A., Wiesner, A., Weinhold, K., Birmili, W., Herrmann, M., Merkel, M., Müller, T., Pfeifer, S., Schmidt, A., and Tuch, T.: Mobility particle size spectrometers: Calibration procedures and measurement uncertainties, *Aerosol Sci. Technol.*, 52, 146–164, 2018.
- Yus-Díez, J., Ealo, M., Pandolfi, M., Perez, N., Titos, G., Močnik, G., Querol, X., and Alastuey, A.: Aircraft vertical profiles during summertime regional and Saharan dust scenarios over the north-western Mediterranean basin: aerosol optical and physical properties, *Atmos. Chem. Phys.*, 21, 431–455, <https://doi.org/10.5194/acp-21-431-2021>, 2021.